npj | advanced manufacturing

Review

https://doi.org/10.1038/s44334-024-00005-w

Multi-material vat photopolymerization 3D printing: a review of mechanisms and applications

Check for updates

Saroj Subedi[1,3], Siying Liu[2,3], Wenbo Wang[2], S. M. Abu Naser Shovon[1], Xiangfan Chen[2] ✉ & Henry Oliver T. Ware[1] ✉

Vat photopolymerization (VPP) is originally considered a single-material process due to cumbersome and time-consuming material switching. Multi-material VPP has been continuously explored with significant switching time reductions realized in recent years, enabling rapid, functional device printing. In addition, VPP hybridization has been explored, enabling printed objects comprising of diverse UV-curable and functional materials. Herein, the authors review the current state of multi-material VPP and VPP hybridization and the remaining challenges.

Additive manufacturing (AM), also known as three-dimensional (3D) printing, typically refers to the manufacturing procedures where 3D computer-aided design (CAD) model data is digitized into a series of two-dimensional (2D) cross-sections with predefined layer thicknesses and successively joined into objects in a layer-by-layer manner[1–3]. 3D printing is thriving as an effective and robust method in fabricating advanced materials and architected, functional devices, and has been significantly utilized in both academia and industry. For example, GE Aviation has a dedicated "Additive" sub-division and has produced over 30,000 fuel nozzle tips via metal-based AM/3D Printing[4]. Depending on the specific methodology, 3D printing is compatible with several categories of materials such as polymers, ceramics, metals, and composites. According to working principles, there are seven major categories of 3D printing processes, including (1) Binder jetting (BJT); (2) Directed energy deposition (DED); (3) Sheet lamination (SHL) (4) Material extrusion (MEX), such as fused filament fabrication (FFF) and direct ink writing (DIW); (5) Powder bed fusion (PBF), such as selective laser sintering (SLS); (6) Material jetting (MJT) such as inkjet printing (IJP), electrohydrodynamic (EHD) jetting, aerosol jet printing (AJP); and (7) Vat photopolymerization (VPP), such as stereolithography (SLA), digital light processing (DLP), projection micro stereolithography (PμSL), and continuous liquid interface production (CLIP)[3,5,6]. Figure 1 highlights many of the aforementioned 3D Printing/AM methods. The VPP process is notably different from the other 3D Printing methods in that its products are selectively cured within a bulk liquid-phase feedstock or "ink". This process utilizes photopolymerization to convert the bulk liquid precursor inks to solid polymeric products[7]. Several advantageous features of VPP include high printing quality (including resolution and surface finish), versatile ink chemistry, and much more limited need of structural supports to create complex structures (refer to "Vat photopolymerization (VPP)")[8].

Currently, VPP has progressed from merely an industrial prototyping method to a pivotal tool for producing parts of production quality. For example, the advent of CLIP has significantly enabled the mass production capabilities of 3D Printing. Adidas and Riddell have partnered with the company Carbon to produce the 4DFWD running shoe midsole and the inner liner for the Diamond helmet platform, respectively[9,10]. Despite this, the adoption of VPP 3D Printing into economically feasible solutions for practical multi-material and multi-functional devices still encounters significant challenges. While VPP is a very mature process and offers high-resolution capabilities, a major limitation is it is commercially considered a singular material process due to its characteristic ink vat. The "vat" houses the material ink and acts as a build chamber for the as-printed object. The necessary switching between multiple inks to enable heterogenous materials and multi-functionality within the final VPP-produced object has posed a major obstacle for mass adoption, but significant progress has been made in this endeavor.

Herein, we report a systematic review of multi-material VPP-based AM/3D Printing. In this review, prevailing VPP-based 3D Printing methods are first introduced and categorized ("Vat photopolymerization (VPP)"). Next, the state of the art of multi-material VPP is introduced, categorized, and evaluated ("Multi-material VPP"). Section "VPP hybridization" will include a state of the art of hybridized 3D printing methods (combining multiple working principles together within a singular printing apparatus) which either incorporates VPP directly or incorporates VPP's selective curing methods (laser beam or digital light projectors). Lastly, the concluding section offers a summary and anticipates future development directions ("Remaining challenges and outlook").

[1]Department of Mechanical and Aerospace Engineering, North Carolina State University, Raleigh, NC, USA. [2]School of Manufacturing Systems and Networks (MSN), Arizona State University, Mesa, AZ, USA. [3]These authors contributed equally: Saroj Subedi, Siying Liu. ✉e-mail: xiangfan.chen@asu.edu; howare@ncsu.edu

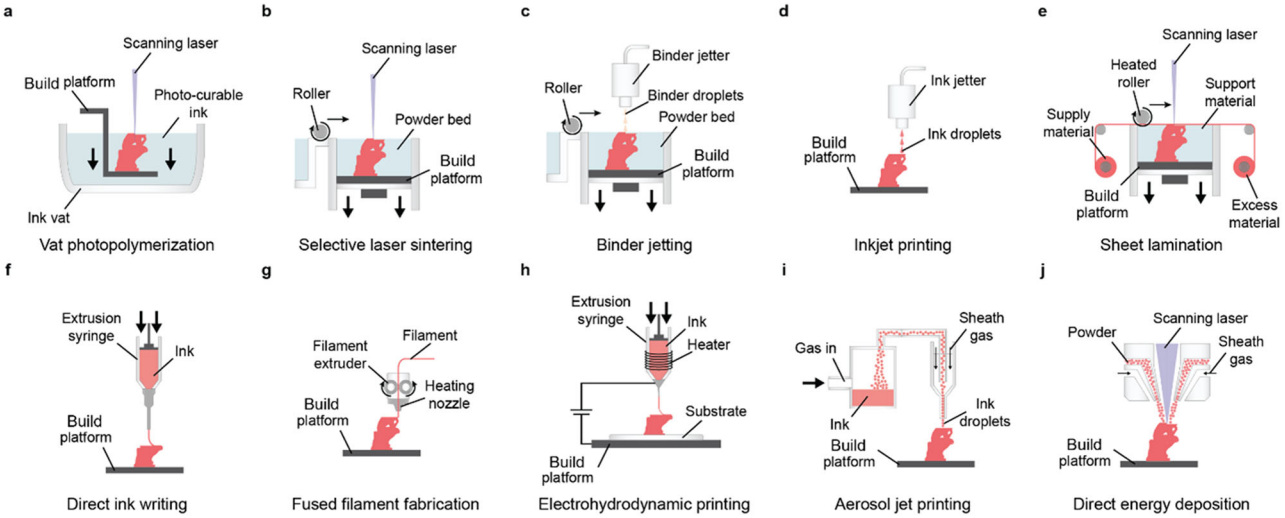

Fig. 1 | Schematic representations of various 3D printing techniques. a Vat Photopolymerization (VPP). **b** Selective Laser Sintering (SLS). **c** Binder Jetting (BJT). **d** Inkjet Printing (IJP). **e** Sheet Lamination (SHL). **f** Direct Ink Writing (DIW). **g** Fused Filament Fabrication (FFF). **h** Electrohydrodynamic Printing (EHD). **i** Aerosol Jet Printing (AJP). **j** Directed Energy Deposition (DED).

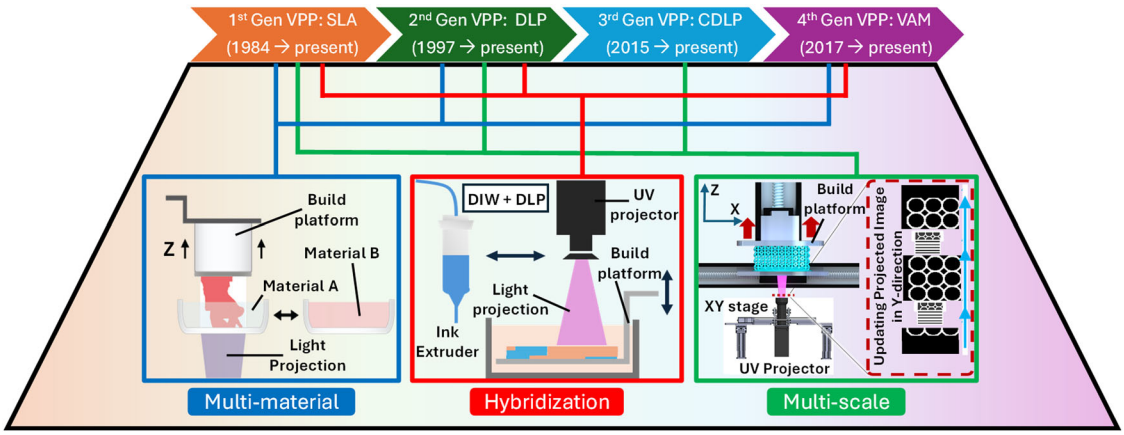

Fig. 2 | Generations of VPP and cross-generational functionalities.

Vat photopolymerization (VPP)

VPP-based 3D printing refers to a subcategory of 3D printing methods, where photo-curable inks are loaded into "ink vats" (also termed "resin baths"), irradiated by light and undergo selective photopolymerization, transforming into solidified parts[11,12]. Photo-curable inks formulated for the VPP typically consist of monomers and/or oligomers, cross-linkers, photoinitiators (to initiate photopolymerization), photo-inhibitors or photo-absorbers (to fine-tune the printing resolution and speed), as well as solvents if necessary (to retain homogeneous dispersions or to reduce viscosities)[13,14]. Additional ingredients can be included for specific applications. For example, functional fillers can be included within the ink to manufacture mechanical/electrical/piezoelectric/magnetic/thermal composites or green bodies for further consolidation[15–21]. Multiple review texts exist which greatly describe the various VPP generations[22,23]. We will, however, briefly describe the pertinent VPP generations with respect to multi-material printing.

VPP, originally represented by stereolithography (SLA), have continuously evolved over the "generations" (Fig. 2 and Table 1) since the first patent filed by Charles W. Hull in 1984[22,24,25]. VPP's 1st generation, SLA, utilizes a scanning laser, typically within the ultraviolet (UV) or blue spectrum to selectively cure the photo-curable ink voxel-by-voxel (minimum fabricable volume unit)[14,26]. Each individual 2D cross-sectional layer is raster scanned by the laser, and each layer is serially stacked in the *Z*-direction until the final object is finished. VPP is well-recognized for its superior printing resolution. This is controlled by multiple factors, including system hardware (i.e., stage resolution, chosen optics, etc.) and ink-specific parameters (ink light absorption, reactivity, rheology, etc.). In detail, the lateral (*X*–*Y* plane) resolution of SLA (in fact, all VPP generations) is predominantly defined by the optical characteristics of the printing apparatus, whereas the longitudinal (*Z*-axis) resolution is affected by both the resolution of the system's *Z*-axis stage and by the Beer–Lambert law within the material ink. The Curing Depth of each layer is closely correlated to the absorbed energy profile by the material ink[14,26]. This absorption is affected by multiple factors such as input light dosage, photoinitiator type and concentration, and any additional photo-absorber[27,28]. Any embedded fillers (i.e., ceramic or metal particles) can act as an additional light absorber and could redirect the incident light laterally (light scattering)[15,29]. High-resolution printing via SLA's raster scanning method can be very time-consuming and have a low overall manufacturing throughput to fabricate tall and/or large-area structures. Similarly, two-photon lithography (TPL), which also fabricates objects via scanning of a single-voxel beam, has a spatial resolution in the nanometer scale by employing the two-photon absorption (TPA) mechanism and is used for very high precision parts, such as microscale optics and biomedical uses[30]. Photoinitiators for TPL absorb two photons

Table 1 | Key VPP "Generations" which have utilized multi-material printing

Vat Photopolymerization				
Generations	Stereolithography (SLA) 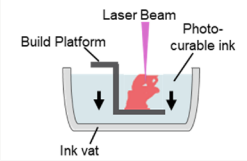	Digital Light Processing (DLP) 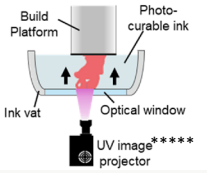	Continuous Digital Light Processing (CDLP) 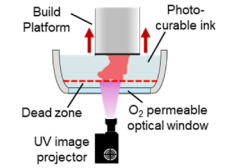	Volumetric Additive Manufacturing (VAM) 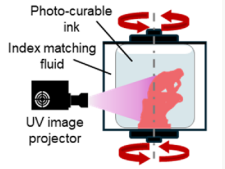
Illumination Method	Laser Beam	Projected Image Exposure	Projected Image Exposure	Projected Image Exposure
Layer-by-Layer Fabrication	Yes	Yes	No, Continuous	No, Continuous
Additional Description	• 2D Layers defined by voxel-by-voxel raster scanning of laser beam. • Scalability dependent on optical system	• 2D Layers defined by image projected onto ink surface with a singular exposure time. • Fabrication area based on projector system and optics. • Trade-off between fabrication area & feature resolution.	• Continuously moving printing platform. • No adhesion occurs at optical window. • Image projection & stage movement are synced.	• Continuously rotating ink container. • Image projection & rotational movement are synced. • Tomographic construction via energy accumulation.
Photo-curable Functional Groups	• Acrylate • Methacrylate • Acrylamide	• Maleimide • Fumarate • Vinyl	• Epoxide • Thiol-Ene ("Click" Chemistry) • Thiol-Yne ("Click" Chemistry)	[14,126]
Fabrication Time Scaling	time $\propto \left(\frac{dimension}{voxel\ size}\right)^3$	time $\propto \frac{Part\ Height}{Layer\ Thickness}$	time $\propto \frac{Part\ Height}{Platform\ Speed}$	time $\propto$ 10s of seconds
Achieved Fabrication Rates	Speed: 31 mm/hr* Volumetric: 1.15×10^5 mm^3/hr** [127]	Speed: 250 mm/hr* Volumetric: 5.8×10^6 mm^3/hr*** [128]	Speed: 430 mm/hr Volumetric: 10^8 mm^3/hr [54]	Speed: 5400 mm/hr Volumetric: 8.6×10^7 mm^3/hr**** [60]

**Reported speed of commercially available printer*
***Estimated by printer system software using test volume and same material/slicing conditions used for reported speed*
****Estimated by multiplying given vertical speed with build size*
*****Values obtained or estimated from Article's Supplementary material*
******Image projectors can utilize UV or visible light wavelengths. VPP inks will typically utilize UV or blue light sensitive photoinitiators.*

simultaneously from a near-infrared (NIR) femtosecond laser and transit from ground state to a higher energy level, namely excited state, triggering the photopolymerization process[31–33]. TPL offers superior nano-scale printing resolution beyond the optical diffraction limit, and each singular voxel possesses an ellipsoidal geometry due to the intrinsic optical nonlinearity[34,35]. While the individual voxels of SLA and to an even greater extent TPL can be very high resolution, the fabrication methods require large amounts of time to create large-scale (centimeter-scale) objects.

Instead of scanning a singular beam to print voxel-by-voxel, digital light processing (DLP) parallelizes the incident light into 2D patterns to print objects layer-by-layer. This approach can substantially enhance fabrication throughput compared to SLA. DLP can be defined as the 2nd generation of VPP. DLP has been referred to by other names in the literature such as mask/image projection stereolithography or (when optics are adjusted for micrometer-scale voxels, also known as PμSL). DLP compared to SLA is a more parallel process, in that, each individual cross-sectional layer is represented as an image that is projected onto the ink surface. Layer fabrication is induced via a singular exposure of the pattern image for a given exposure time. In this process, the incident light into the liquid ink is patterned via a spatial light modulator, which may be based on a digital micromirror device (DMD) or liquid crystal on silicon (LCoS). An additional capability of DLP is the ability to impart gradient illumination, enabling finer control of feature resolution and localized gradients of crosslink density[36–38]. TPL has also seen significant strides in throughput from its introduction. Efforts made to improve the throughput of TPL mainly rely on parallelization based on projection or diffraction optics[39,40]. There have been notable examples of parallelized TPL in recent years. Hahn et al. prototyped rapid multi-focus TPL based on fully customized diffractive optical element. The authors adopted Gerchberg and Saxton algorithm for optimized design such that the diffractive optical element consisted of square pixels with a side length of 2 μm and eight varying height levels, and it could split the laser beam into nine beamlets for parallelization[39]. Saha et al. developed a femtosecond projection TPL (FP-TPL) technique by integrating a DMD-based projector into the voxel-by-voxel TPL system. They succeeded in spatially and temporally focusing the femtosecond laser for layer-by-layer parallelization. FP-TPL enables the increment of printing throughput up to three orders of magnitude without sacrificing either desired geometric complexity or line widths less than 157 nm[40].

While DLP significantly increases the manufacturing throughput from SLA, its fabrication time is still hampered by layer delamination, recoating, and transition time between fabrication layers. This makes centimeter-scale prints require several hours for printing parts with sub-100 micrometer layer slicing thickness[41]. To address this imperative issue associated with SLA and DLP, the 2010s saw the introduction of VPP's 3rd generation, which can be very generally described as continuous DLP (CDLP). CDLP was first introduced by Tumbleston et.al. as continuous liquid interface production (CLIP), which utilizes a transparent oxygen-permeable window at the bottom of the ink vat in the incident light path[42]. This enables oxygen to diffuse into the photo-curable ink and form a thin, oxygen-dense region called a "deadzone", within which photopolymerization is inhibited[42]. The employment of oxygen inhibition layer in the CLIP process can eliminate the delamination and recoating steps present in SLA and DLP, which enables continuous photopolymerization during the process. As a result, the printing speed has significantly increased, and the printed products show smooth surfaces, isotropic mechanical properties, and diverse printable material options[43,44]. As a result, CLIP has come to be known as Digital Light

Synthesis (DLS) in an industrial context, which has been applied in various commercial sectors. Building on this platform technology, various groups have developed innovative methods to further strengthen the capability of CLIP. For example, to enable high-speed fabrication of 3D structures containing microscale features at a fast-printing speed, DeSimone, Sun, and Chen research groups, as well as several others, have established a customized μCLIP process, pushing the printing resolution down to the microscale (e.g., 1–10 μm voxel resolution)[45–51]. In parallel, another method which enables continuous fabrication was introduced through rapid mass transport via a moving immiscible fluorinated oil interface. This approach creates a non-stick optical quality surface that rapidly removes heat from the print area and replaces as-cured material and with fresh material ink to enable continuous printing known as high-area rapid printing (HARP)[52,53]. An additional notable method utilizes two light wavelengths to concurrently create a polymerization inhibition layer while enabling photopolymerization to occur above that inhibition layer[54]. In general, the CDLP processes (i.e., CLIP/μCLIP, HARP, inhibition patterning) eliminate the delamination/translation step from standard DLP, which brings the fabrication speeds into the range of 100–1000 s of millimeters per hour[42,52,54,55]. Parts with high-resolution feature requirements that would normally take more than 10 hours to print via SLA or DLP can be made with CDLP in a single hour or even within a few minutes, depending on the ink's reactivity and rheology[41,42].

More recently, volumetric additive manufacturing (VAM) is emerging as a new "generation" of VPP that deviates from the voxel-by-voxel or layer-by-layer process. Instead, VAM is achieved utilizing one or multiple superimposed optical profiles that simultaneously solidify the entire 3D object[56,57]. As the most representative VAM method, Kelly et al. developed computed axial lithography (CAL) based on tomographic reconstruction[57]. In CAL, the photo-curable ink inside the ink vat (in this instance, a rotary vial) is solidified via a set of 2D projections, each propagating through the ink at different angles, so that the superposition of these exposures results in a volumetric dosage profile corresponding to the designed geometry. As a layer-less and support-free fabrication method, despite offering high throughput manufacturing of 3D objects, it is challenging to establish quantitative correlations between printing speed (typical time durations for centimeter-scale objects are tens of seconds) and printing resolution (80 μm for positive features and 500 μm for negative features in acrylate materials) for CAL[58]. Printing resolution of VAM is limited by several physicochemical parameters, with optics playing the essential role since the smallest features in VAM are defined by the superpositions of optical profiles from different angles[57–59]. Up to now, the printing resolution of VAM is still not as fine as those of other VPP generations, but researchers have been dedicating themselves to yield improvements both theoretically and experimentally[60,61].

While the generations of VPP are described in terms of manufacturing throughput, significant cross-generational strides in functionality have been made (Fig. 2). This includes multi-material fabrication, hybridization, and multi-scale fabrication capabilities. Multi-scale fabrication is outside the scope of this review; however, briefly, this would include parallelization of TPL (projected image)[39,40] and expanding the fabrication area of microscale focused DLP (PμSL) via optics or translational stages[62–64]. Since 2001, multi-material fabrication has been performed in research with significant strides made in material switching time and efficiency of material usage[37,65–67]. Multi-material printing with VPP has been demonstrated in all of the described VPP generations and performed via "(i) Multiple Vat Switching", (ii) "Single Vat with Dynamic Fluid Delivery", and (iii) "Unpatterned Ink Deposition 'Vat-Less' VPP". From the 2010s to now, VPP has additionally been explored in combination in a fully automated configuration with other 3D printing processes to enable even greater capabilities for the printing of multi-material functional devices. Multi-material printing with VAM is represented via a hybridized printing process[68]. These "hybridized" fabrication approaches enable non-photo-curable materials or highly viscous inks/slurries to be efficiently implemented within the multi-material object build.

Notably, aside from multi-material VPP achieved by utilizing multiple, distinct photo-curable inks, VPP 3D printing of anisotropic/gradient materials via localized control over a singular photo-curable ink has also been recognized as multi-material 3D printing as it leads distinctively localized material properties. To achieve this, localized, in situ control is applied to the photo-curable inks during the 3D printing procedures, which typically falls into two subcategories. The first strategy is achieved via the localized, spatially programmable orientation alignments of material constituents (such as liquid crystalline mesogens) or embedded fillers that exist in diverse 0D (spherical particles), 1D (rods, tubes and wires) and 2D geometries (platelets and flakes), granting tailorable anisotropic properties[69,70]. To attain such controllable alignment, external stimulus such as mechanical shear, geometrical confinement, or electrical/acoustic/magnetic field is incorporated into the VPP 3D printing apparatus. The second strategy is enabled via the usage of a spatial light modulator which can be programmed to project grayscale images for localized control over the exposure time and light intensity so that localized/gradient properties can be attained. This in turn leads to the precise control over localized degree of photopolymerization, which is correlated to the mechanical properties of 3D-printed parts[71]. Nevertheless, the above-mentioned strategies are beyond the scope of this review article and will not be thoroughly discussed.

Multi-material VPP

Multi-material VPP has been around since the turn of the century since Maruo et al. printed multiple polymeric material waveguides via VPP in 2001[67]. Most of "Multi-material VPP" will be devoted to how material inks are switched and the strides that have been made in improving throughput. Multi-material VPP has been utilized for notable applications such as soft robotics[72], soft actuators[65], novel mechanical metamaterials[73], bioprinting[74], and flexible sensors[75]. Several of these instances are shown in Fig. 3.

Multiple vat switching enabled multi-material VPP

To enable the integration of different materials comprising distinct functionalities in a single 3D object, one intuitive and traditional approach is to employ multiple containers/vats, each containing a specific printable ink or cleaning solvent (Fig. 4a). Typically, the switching is enabled via linear translation of the ink vats or via a rotating carousel of vats. These vats can be manually or automatically switched, allowing use of different photo-curable monomer combinations within the final product. However, this material switching method does require considerable time (in situ) dedicated to (Step 1) physically exchanging vats, (Step 2) removing excess uncured inks from the print to prevent cross-contamination, and (Step 3) drying the objects to prevent material dilution with solvent. Step 2 (the "cleaning step") can include wiping the print with an absorbent cloth/pad or rinsing the excess material away after each switching instance. Step 3 (the "drying step") can include passive or active drying. "Passive" drying is simple ambient air drying, and "active" drying utilizes fans or air jetting, for example. These "Steps" significantly hinder this method's throughput, especially if the object has multiple materials in the same cross-sectional layer. The overall system setup such as system "orientation" and placement of vats, cleaning, and drying stations within the system can greatly affect total process time. VPP printing systems (with the exception of VAM) are configured as either Top-down or Bottom-up "orientations" (Table 2). The system orientation significantly influences the implementation of the Multiple Vat Switching process for multi-material printing.

The earliest reported Multiple Vat Switching implementation utilized the Top-down orientation in the automated "Vat Carousel" method in 2004[76]. This method employed four different vats of materials on a rotary platform, with the build platform raising up during vat changes. In addition, Arcaute et al. reported a manual mini-vat switching system, albeit requiring more time for removing excess inks and drying[77]. Table 2 lists notable advantages and disadvantages of Top-down and Bottom-up oriented systems. Because of the noted drawbacks in Top-down systems, Bottom-up systems have drawn more favor in recent years for Multiple Vat Switching. The first iteration of Bottom-up systems in multi-material VPP was introduced by Zhou et al., utilizing a rotating platform consisting of two vats with cleaning and drying steps[78]. Beyond system orientation, the arrangement of the ink vats and any cleaning and drying stations within the system can

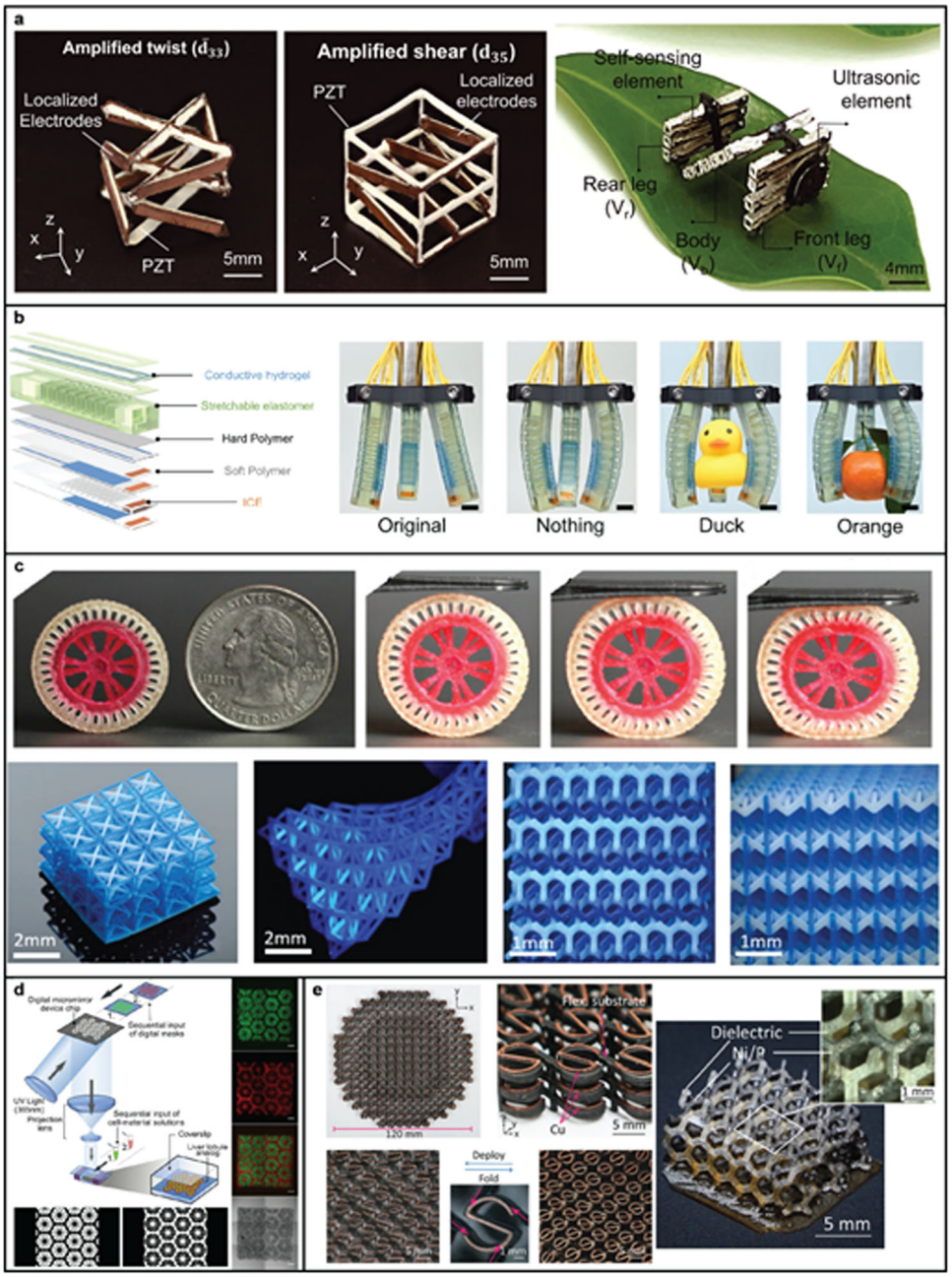

Fig. 3 | Applications of multi-material VPP. **a** Piezoelectric metamaterials for programmable piezoelectric responses and stimuli-responsive multi-modal mobile microrobot, (Image reproduced with permission from ref. 72, Copyright AAAS, 2022). **b** Schematic and actuating performance of a MM VPP 3D-printed soft pneumatic actuator comprising multiple sensors, (Image reproduced with permission from ref. 65, Copyright Springer Nature, 2022). **c** Mechanical metamaterials and structural components obtained via MM VPP 3D printing (images reproduced with permission from ref. 105 and ref. 73, Copyrights John Wiley & Sons, Inc., 2023 and Springer Nature, 2018, respectively). **d** MM VPP 3D bioprinting of hydrogel-based hepatic construct, (Image reproduced with permission from ref. 74, Copyright National Academy of Sciences, 2016). **e** MM VPP 3D-printed lightweight and deployable antenna system, (Image reproduced with permission from ref. 75, Copyright John Wiley & Sons, Inc., 2024).

affect the efficiency of the process. To alleviate the long material switching time (~180 s) and increase material switching frequency, Matte et al. introduced a vertical material ink vat storage system for storage of up to eight different materials. They utilized this vertical storage system in combination with translational motion for bringing the intended vat into the printing region instead of full system rotation or linear translation switching mechanisms[79]. The cleaning process in this method was performed concurrently while material switching was ongoing, thereby reducing the total switching time. The process of physically changing the location of the vats through translation or rotation can make the printing process unstable as the large volume ink vats now must move after every layer of the print. Jiang et al. addressed this challenge by utilizing fixed vats with rotational movement of the build platform rather than moving the ink vats[80]. In their design, placing the cleaning system vat in the middle of the ink vats minimized the traveling distance of the build platform during switching. Similarly, Hu et al. adopted a fixed vat strategy which used linear translation of the build platform, instead of rotation[81]. Another notable vat switching approach by Huang et al., utilized a 6-degree-of-freedom robotic arm and translational vat switching[82]. This approach also utilized μCLIP and when combined with the 6-DoF capability of the build platform was able to rapidly create multi-material off-axis parts continuously.

From the early iterations of the Multiple Vat Switching method to the present day, research attention has emphasized both efficient switching and effective cleaning/drying (Step 2/Step 3) after every layer to improve fabrication throughput. Step 2 and Step 3 are *just as important* to enable or hinder high throughput for multi-material VPP. The cleaning/drying sequences within the overall exchange process can require as much as 2–5 min for every vat switching command[78,83,84]. Generally, the cleaning process (Step 2) of residual ink on the printed object and build platform improved simultaneously with the switching system upgrades. From the inception of multi-material VPP, part cleaning was performed by rinsing the object in alcohol[76,85,86] or in distilled water[77]. However, this contaminates the printed object with the cleaning agents and requires idle time in the print for drying. Another early multi-material VPP cleaning mechanism was to

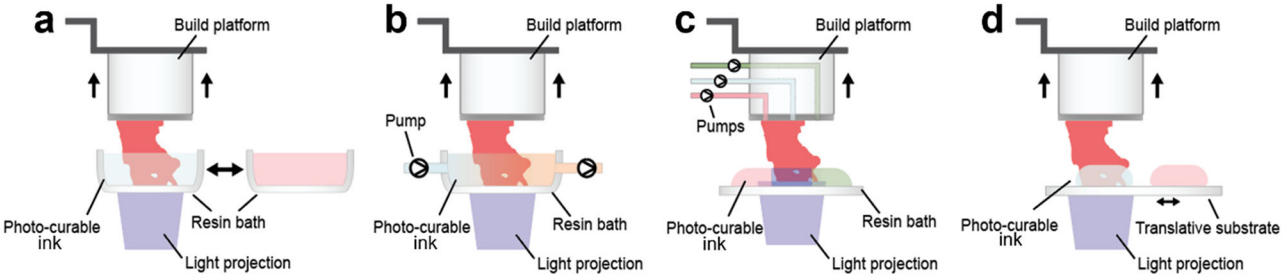

Fig. 4 | Schematics of common approaches to multi-material VPP processes. a Multiple vat switching. **b** Single vat with dynamic fluid delivery. **c** iCLIP, a specific method of single vat with dynamic fluid delivery. **d** Unpatterned ink deposition, "Vat-less" VPP.

Table 2 | VPP system orientations that are present in SLA, DLP, and CDLP

System orientation	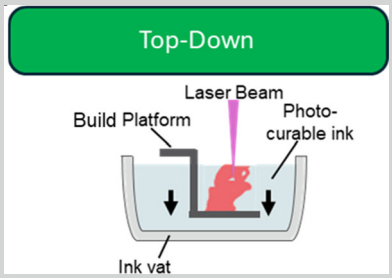	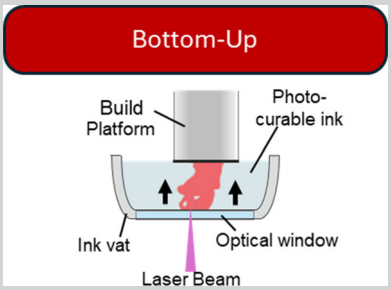
Illumination	Top of ink surface	Bottom of ink vat
Build platform	Lowers into ink vat during print	Raises out of ink vat during print
Additional description	• Curing occurs at ink/air interface, typically (free surface) • Ink must "recoat" the previous layer and flatten before printing can resume.	• Curing occurs at ink/window surface (constrained surface) • Object must be "delaminated" from optical window and ink recoated before printing can resume.
Advantages for multi-material printing	• More fabrication sequence options due to printing platform being able to return to earlier build layers. • Whole volumetric regions of distinct materials can be printed at a time[85].	• Object height determined by total ink volume in vat. • Requires less prepared material ink for printing tall objects.
Disadvantages to multi-material printing	• Object height limited by height of ink in container. • Requires more prepared ink for tall structures compared to Bottom-up	• Switching *must* occur every instance of multiple materials in same cross-section, unlike Top-down.

wipe the part using absorbent wipes or a soft brush[77,78]. The wiping method is fast, although it does not clean the ink residue completely and requires an additional rinsing mechanism. In 2013, Zhou et al. first implemented the ultrasonic cleaning method with an alcohol-based cleaning agent during the rinsing process[78]. However, this method leads to unwanted bubbles to remain on the part's surface, which will affect print quality without the addition of an air drying step (Step 3)[79]. Later, Step 2 was improved using a spray mechanism, which is more environmentally friendly and saves time compared to earlier methods. In addition, to further increase the fabrication throughput, Step 3 was augmented via active drying mechanisms such as a blower fan or compressed air have been utilized[79–81]. In 2019, Matte et al. used sprinkler nozzles and a pump to spray the part with alcohol solution and dry it with a fan, which in total only required 15 s for cleaning/drying[79] compared to 120 s by Zhou et al.[78]. In addition, fabrication area of the work was quite large: ~30.5 × 15.25 cm^2, showcasing high scalability potential[79]. Similar cleaning mechanisms were utilized by Hu et al. and Jiang et al., which also showcased very low cleaning times (~18 s and lower)[80,81]. Another notable approach of cleaning and drying was recently made by Cheng et al. in 2022 by rapidly spinning the build platform at 3000–6000 rpm. The induced centrifugal force enabled full switching/cleaning sequence to reduce to within 30 s[65].

While cleaning/drying method described by Matte et.al. was very rapid, the described vat switching approach (Step 1) ultimately kept the total switching time high at 62 s. Hu et al. and Jiang et al. who used similar cleaning/drying methods additionally utilized efficient and strategic build platform motion during the material switching step, which would potentially keep the total switching time relatively low. The total switching times, however, are not stated in those works. Due to the close placement of ink vat and cleaning station in Jiang et al., it is likely that the (Step 1) switching time between materials is effectively negligible. The combination of effective system arrangement and effective cleaning and drying make the system shown by Jiang et al. have very high scalability and commercialization potential. The Cheng et.al. centrifugal cleaning method was shown to be applicable to ceramic-infused inks with 6000 mPa·s. Cheng et al. also state it could handle material inks up to 10,000 mPa·s although rotational speed would need to be increased[65]. These viscosity values are among the highest tested across all multi-material VPP approaches. In terms of viscosity range, this centrifugal cleaning approach was shown to be able to handle low-viscosity and high-viscosity inks. While the centrifugal cleaning method did require a higher overall switching time than the cleaning spray and active drying methods, it does not utilize solvents, which could improve overall print quality. In addition, the fabrication area in the work was shown to be 13.0 × 18.0 cm^2, showcasing large scalability potential. Reduction of total switching/cleaning/drying times to the 15–30 s range greatly improves the viability of the VPP process for multi-material functional devices and later commercial adoption. Table 3 shows a summary of material exchange

Table 3 | Consolidated literature regarding material exchange system, orientation, cleaning mechanism, and required cleaning time and references

Material exchange	Switching apparatus	Print orientation	Cleaning approach	Cleaning description	Cleaning/switching time or combined (if mentioned)	References
Multiple vat switching	Manual switching	Top-down	Manual cleaning (rinse, wipe and/or air dry)	Distilled water, rinse and wipe with Kimwipes	Not mentioned	77
				Ethanol and autoclaved water rinse three times and compressed air drying	Not mentioned	125
	Rotary switching	Top-down	Manual cleaning (rinse, air dry)	Alcohol/isopropanol rinse, air dry	Not mentioned	76,85,86
		Bottom-up	Automated cleaning (rinse)	Phosphate-buffered saline (PBS) solution rinse	Not mentioned	126
			Automated cleaning (ultrasonic bath, wipe and active dry)	Two brushes (wipe), alcohol solution in ultrasonic bath to clean, and fan drying	~180 s (cleaning)	83
				Soft brush (wipe) and isopropanol solution in ultrasonic bath to clean and fan drying	120 s (cleaning); 180 seconds (switching)	78
			Automated cleaning (wipe and active dry)	Two brushes and cotton pad wipe to clean, and fan drying	~120 s (combined)	83
				Sponge wipe to clean and fan drying	39.9 s (combined)	127
			Automated cleaning (nozzle spray solution and active dry)	Nine spray nozzles containing alcohol and air (clean/dry)	<18 s (cleaning)	80
	Translational switching	Bottom-up	Automated cleaning (rinse)	Isopropanol solution in ultrasonic bath to clean	300 s (cleaning)	84
			Automated cleaning (nozzle spray solution and active dry)	Nine nozzles with surfactant solution to clean and hot air drying	18 s (cleaning)	81
				Three sprinkler nozzles and a pump to clean with isopropanol solution and fan drying	15 s (cleaning); 62 s (switching)	79
			Automated Cleaning (Spinning)	Build platform rotated at 3000–6000 rpm to remove ink residue by centrifugal force	30 s (cleaning/drying)	65
Single vat with dynamic fluid delivery	Pump-based enclosed vat	Top-down	Automated cleaning (withdraw pump)	Residual ink withdrawn by pump followed by flushing with new ink.	2–20 s (switching)	88
		Bottom-up				87
	Pump-based open vat	Bottom-up	Automated cleaning (withdraw pump)	Residual ink withdrawn by pump followed by rinsing with cleaning solvent.	>60 s (switching/cleaning)	89
			Automated cleaning (rinse, dry and wipe)	Residual ink withdrawn by pump followed by rinsing and drying. Platform wiped with brush.	10 s (cleaning)	73
	Injection continuous printing		No cleaning required	Selectively introduces different inks into build area through ink supply channels within printed object.	N/A	66
"Vat-Less": unpatterned ink deposition, selective curing	Rotary switching	Bottom-up	Automated cleaning (rinse, wipe)	Ethanol rinse to clean and wiped with cotton pads	Not mentioned	91
	Translational switching	Bottom-up	Automated cleaning (wipe)	Tissue wiping to clean	Not mentioned	93
			Automated cleaning (rinse, active dry)	Ethanol rinse to clean and air jet-dried	20 s (cleaning)	90
			Automated cleaning (air jetting)	Used 0.5 MPa air jet blast through 2 mm diameter tube	5 s (cleaning)	92,94
				Air jetting to clean/dry	1.5 s (cleaning); 3 seconds (switching)	37

methods, switching apparatus, cleaning descriptions and switching/cleaning/drying process time for all described methods in "Multi-material VPP".

Single vat with dynamic fluid delivery multi-material VPP

While multiple vat switching is the most populous method of multi-material VPP, other approaches have been explored. From the standpoint of fabrication efficiency, the capability to conduct multi-material printing within a single vat presents an ideal scenario, as the number of moving components is reduced. This approach can substantially reduce fabrication times by allowing the vat to remain stationary while facilitating the injection and extraction of inks via fluid delivery systems. A schematic denoting the general methodology of this method is shown in Fig. 4b. Pumps play a major role in this fabrication approach. Notably, in 2018, Chen and Zheng pioneered a novel approach to Single Vat multi-material DLP printing process by introducing a system that employs serial programmable ink feedstocks (product shown in Fig. 3c, bottom image)[73]. This innovation enables automated supply of diverse inks into the vat. The ink switching process is efficiently executed by initially removing residual material with a brush, followed by automated perfusion of the new ink, minimizing cross-contamination through drying. The system's automated design enabled the successful fabrication of metamaterials with customizable negative Poisson's ratios, incorporating materials of varying stiffness, as shown in Fig. 3c. Miri et al. also presented an novel method that enabled rapid material switching through the use of an enclosed microfluidic chip as the print chamber, in 2018[87]. This system employs Bottom-up DLP, printing onto a flexible membrane. The confined volume within the chamber ensures efficient replacement of the old material ink with newly injected ink. By precisely controlling the flushing duration and flow rate, material switching can be achieved without the need for a cleaning solvent. Although this technique allows for the swift fabrication of multi-material 3D objects, it is important to note that the maximum achievable height of the printed objects is limited to a few millimeters[87]. In the subsequent year, Han et al. introduced an enhancement to the enclosed multi-material printing chamber, incorporating a piston-like mechanism to extend the printing height, potentially, although it was not stated what the maximum height could be[88]. Diverging from earlier methodologies, this configuration employs a Top-down DLP (although it uses an optical window as a constraining surface) and adds an additional outlet at the ink chamber's base, facilitating efficient expulsion of residual ink during material transitions. Beyond the successful creation of polymer objects, this innovation enabled the production of composite materials loaded with ceramic and metal particles. Nonetheless, the complexity of this system's design, necessitating precise manufacturing for the piston-like chamber, poses significant challenges for widespread replication. In 2023, Quero et al. disclosed a more straightforward, yet effective, strategy for achieving multi-material printing within a single vat on a commercial DLP printer[89]. This method incorporates peristaltic pumps into a standard vat for the evacuation of old ink, followed by the injection of a solvent to clean the vat and the previously printed object, and finally, the injection of new material ink. Moreover, the integration of a tilting mechanism allows the ink bath to pivot toward a side corner, enhancing the removal of residual ink and simplifying the cleaning process. Although the material transition and cleaning durations are lengthier compared to those of the enclosed chamber technique, this approach offers a cost-efficient and easily replicable solution.

While the single vat multi-material strategies have notably enhanced fabrication efficiency compared to traditional multi-vat methods, the production of multi-material objects still requires considerably more time than single-material fabrication. Addressing this, Lipkowitz et al. introduced Injection CLIP (iCLIP, Fig. 4c), a technique falling within the CDLP printing category, which builds upon the foundational CLIP technology[66]. iCLIP stands out for its ink injection flow channel design, essential for optimizing high-efficiency, continuous 3D printing in a single vat. iCLIP features an intricate injection system that precisely delivers diverse inks to the print area, enabling seamless material transitions through a network of controlled valves and channels. This configuration ensures precise material supply, minimizes ink mixing, and preserves material integrity. Notably, iCLIP advances continuous printing technology, significantly reducing fabrication time, which is ideal for rapid prototyping or mass production of multi-material items. Moreover, this method not only expedites production but also improves object quality and consistency. The integration of ink flow control with continuous printing represents a significant stride in VPP, enhancing the process's efficiency and versatility. It is also important to highlight that the design of the fluidic channels is critical for the system's ability to handle materials with a broad range of viscosities. Achieving this involves sophisticated fluidic channel design for varying flow profiles according to the specific viscosity and printing requirements of each ink. The strategic placement and proper sizing of these channels within the print are essential for maintaining a continuous ink supply and facilitating rapid material switches without compromising print speed or quality. By managing such a variety of viscosities, iCLIP is capable of producing parts with enhanced structural strength and tailored functionalities, which are crucial for industries needing robust, versatile components. Notably, iCLIP has successfully printed multi-material 3D objects using high-viscosity inks up to 6500 mPa·s and inks loaded with 1 wt.% multi-walled carbon nanotubes (MWCNT). This is the maximum viscosity shown within Single Vat with Dynamic Fluid Delivery approach. Other listed methods under this multi-material VPP approach utilized a maximum ink viscosity of 700 mPa·s[89]. However, the necessity for precise channel design in each project underscores the need for ongoing enhancements in the precision and adaptability of Single Vat multi-material VPP 3D printing technology.

Unpatterned ink deposition enabled "vat-less" multi-material VPP

From the inception of multi-material VPP, concerns regarding material conservation, cross-contamination, and the time required for material switching/cleaning/drying have been prominent. To address these concerns, in recent years the idea of "Vat-Less" multi-material VPP has arisen. This approach aims to eliminate the dedicated container used in SLA or DLP, while maintaining the usage of a laser beam or a projected image to crosslink the material at high resolutions[90–92]. As long as there is sufficient ink volume for single-layer creation present in the build area, the patterning methods of SLA and DLP remain valid for the process to continue. In terms of material exchange methodology, this approach is most akin to our previously described Multiple Vat-Switching method (section "Multiple vat switching enabled multi-material VPP"). As illustrated in Fig. 4d, in this "Vat-Less" approach, ink "puddles" are deposited onto an optically clear substrate, where the intended material is then rotated or translated into the printing region for fine-feature photopolymerization. The printer system for this material switching method is strictly Bottom-up orientation, which combined with discrete ink puddles further reduces the necessary volume of material for printing[90–92].

This fabrication method has been reported for multiple applications, such as for negative thermal expansion mechanical metamaterials, pneumatic actuators for soft robotics, stretchable hydrogels[37], and multi-colored optics[90]. Like the multiple vat switching method, there needs to be a dedicated material cleaning step to prevent material cross-contamination between the distinct ink puddles. Multiple cleaning methods have been reported, such as wiping via absorptive pads[93], solvent bath with absorptive pads[91], pressurized air jetting[37,92,94], and solvent bath with air drying[90]. The pressurized air jetting between material switching has proven to enable a much more rapid fabrication approach when working with low-viscosity materials, where 1.5 and 5 s air blasts are sufficient to remove uncured ink and prevent cross-contamination of materials[37,92]. The reported viscosity of the utilized material inks in this multi-material VPP approach is 120 mPa·s or lower, which is the lowest of the other multi-material VPP approaches[94]. The combination of pressurized air jetting and a solvent bath can potentially be applicable to more viscous inks, although the cleaning and switching times will necessarily increase[90]. Objects having both low and high-viscosity material inks in the same object could be potentially problematic with this fabrication approach. While "Vat-Less" multi-material VPP has been

shown to be effective for small-part fabrication, it has not yet been utilized for large-area prints in the lab setting. This typical fabrication approach would fall under the microscale-focused DLP category (PμSL) for generally smaller structures[90–92,95]. The scalability of this material exchange approach remains a question, as this approach would then require a larger material ink volume and larger area to clean.

In all three listed multi-material VPP approaches, significant strides have been reported with switching/cleaning/drying times in the lab setting, making them much more viable for potential commercialization. Due to the challenges stated with multi-material VPP in terms of switching time and cleaning/drying concerns of low-viscosity inks, multi-material 3D printing in a commercial setting would employ the deposition-based 3D printing processes (FFF, DIW, or UV-assisted IJP). Multi-material VPP is quite uncommon in the commercial setting. To the authors' knowledge, there are only two commercial multi-material VPP systems, both of which utilize high viscosity, high solid-loading photo-curable slurries containing ceramics or metals. The commercial system from Lithoz (CeraFabMulti 2M30), utilizes Multiple Vat Switching multi-material VPP to create multi-material ceramic/ceramic or ceramic/metal parts[96]. The other commercial system from Admatec (Admaflex 300, which can be configured as a Multi-Material option) would fall under "Vat-Less" multi-material VPP category. Ceramic or metal slurries are deposited and flattened into a uniform thickness layer onto a foil substrate (tape casting) which is then translated into the illumination area and photopolymerized via a DLP projector[97,98]. It is not stated for either system how cross-contamination of material inks is handled. Because the photo-curable inks are high solid loading and high viscosity and the final printed objects are sintered, cross-contamination is possibly considered negligible in these contexts. Commercial multi-material VPP systems for comparatively low-viscosity inks are not available to the authors' knowledge. "Vat-Less" multi-material VPP, with its utilization of unpatterned material deposition and fine-feature printing via high-resolution photopolymerization represents a partial hybridization of printing working principles. Section "VPP hybridization" will highlight hybridization of multiple 3D printing modalities combined with VPP or the use of selective curing illumination (laser beam or DLP projector). This hybridization of printing processes can be scalable to larger areas, while maintaining some of the key advantages of VPP patterning methods.

VPP hybridization

Despite VPP's advantages and the more rapid material exchange methods outlined in Section "Multi-material VPP" for creating multi-material parts, VPP still faces limitations, such as, material being restricted to photo-curable inks. Moreover, the requirement for the material ink to have sufficient flowability or to have specific ink-recoating mechanisms for subsequent layers imposes additional restrictions on the viscosity of usable materials. Conventionally, VPP technology has been limited to materials with viscosities below 10 Pa·s (10,000 mPa·s or 10,000 cP) with many not reaching above 3 Pa·s (3000 cP)[99,100]. High molecular weight monomers/oligomers, and high solid loadings of inorganic fillers such as ceramic/conductive micro/nanoparticles increases the ink viscosity, but the ability to produce parts with high resolution is still desired[99]. Hybridization of multiple printing modalities aims to overcome the individual process limitations, while enhancing versatility and efficacy. This section delves into hybrid 3D printing techniques, combining VPP patterning methods (laser beams or DLP projectors) with other 3D printing technologies.

DIW can extrude materials with viscosities up to 1350 Pa·s, as long as the ink exhibits non-Newtonian "shear-thinning" rheological behavior[101]. DIW is material agnostic, in that, it offers the ability to print materials that are subject to many solidification mechanisms, not just photopolymerization. However, DIW materials should have a relatively large viscosity, as lower viscosity would impede the ability to maintain the deposited shape until solidification. In addition, the resolution of the process is constrained by the nozzle diameter, making it significantly less precise than VPP-based processes. FFF, another extrusion process, also has its resolution constrained by its nozzle diameter. FFF's primary feedstocks are thermoplastic filaments, which are subject to melting and re-solidification. For material jetting, AJP can handle fluids with viscosities up to 1 Pa·s, while IJP can typically only handle very low-viscosity fluids, up to 20–30 mPa·s[102]. IJP additionally deposits droplets of very low volumes (in the picoliter scale). The various process differences in rheology requirements, feedstock material types, resolution differences, and printing mechanisms are collected in Table 4. Integrating another 3D printing process with VPP can be challenging and lead to issues such as layer mismatch, material contamination, weak interfacial bonding, undesired anisotropic properties, mismatched post-processing requirements, and surface finish disparities.

Although not all noted challenges have been explicitly explored, there are notable instances where researchers have attempted to better understand VPP hybridization and mitigate these challenges. For example, Peng et al. have addressed the layer mismatch problem by printing eight DLP layers for every two DIW layers[103]. To understand interfacial bonding in VPP hybridization, they additionally analyzed the interfaces of DIW-printed conductive ink and DLP-printed elastomer matrix using SEM and tensile measurements. In this case, the DLP and DIW inks were both acrylate-based, highlighting the need to choose complementary material inks/feedstocks in hybrid printing. Materials with different surface energy and chemical compatibility such as thermosets for DLP with thermoplastics for FFF have weaker interfacial bonds due to interdiffusion complexities[104]. Comprehensive studies on the curing kinetics for any chosen hybrid processes and the interaction of their curing mechanisms are necessary to achieve robust interfaces. Similarly, how the processes interact during printing is important. For instance, depositing DIW ink directly onto VPP-printed objects can hinder proper bonding due to oxygen inhibition. Jie et al. tackled this by dispensing DIW ink *inside* the uncured DLP-ink matrix, which also aided shape retention through surface tension between the two inks[105]. On the other hand, the thermal properties of materials, including their thermal expansion coefficients and heat transfer characteristics, can also significantly affect hybrid printing. Mismatched thermal properties between different layers or components can lead to internal stresses, warping, or delamination, compromising mechanical performance and durability. Therefore, it is crucial to study the combination of materials and synchronize the nuances of different processes to achieve successful hybridized fabrication of multi-material parts. Figure 5 showcases several hybridized systems which include VPP that have been reported. Table 5 summarizes the reported VPP hybridization methods. Importantly, we note where manual intervention or full automated hybridization was realized.

From our comprehensive review of recent literature, it becomes evident that the integration of DLP with DIW is the most extensively explored VPP Hybridized printing technique, showcasing its widespread adoption and utility in both 3D and 4D printing applications[99,103,106–108]. This hybrid approach typically employs DIW for the deposition of conductive inks, while DLP is utilized to cure the deposited feedstock and ink within the vat, facilitating the fabrication of functional composites with adjustable mechanical properties, improved interfacial bonding, and multi-functionality. The earlier instances of VPP/DIW hybridization were primarily developed for electronics printing. Palmer et al. was the earliest reported work in 2005 which involved manually transferred parts between SLA and DIW machines to fabricate three-dimensionally interconnected circuits[109]. This was further refined by Lopes et al. by integrating SLA and DIW processes within a singular machine[110]. However, this hybridization still required intermittent halts to manually clean ink slots and insert electrical components. The 3D circuits fabricated by this group as shown in Fig. 6a still necessitated manual deposition of ink between printing stages[111]. Taking a slightly different approach, Vatani et al. fabricated tactile sensors by first shaping parts using DLP and injecting conductive ink into pre-formed channels, which still required manual assembly for functional completion, although DLP and DIW modules were integrated into one apparatus[107]. This methodology has evolved from requiring significant manual involvement toward greater automation. Peng et al. demonstrated the capability of this combination to produce multi-color parts (Fig. 6b), strain sensors, and soft robots (Fig. 6c), highlighting the broad compatibility with various inks.

https://doi.org/10.1038/s44334-024-00005-w

Table 4 | Comparison of various 3D printing processes

Process	TPL	SLA	DLP	VAM	DIW	FFF	IJP
Description	Utilizes a femtosecond laser to induce polymerization via simultaneous absorption of two photons	2D layers defined by voxel-by-voxel raster scanning of laser beam onto photo-curable ink surface	2D images projected onto the photo-curable ink surface to cure layer via a single exposure	Entire 3D object created by irradiating a volume of photo-curable ink from multiple angles	2D layers defined via extrusion of a viscoelastic ink through a single-point fine nozzle	2D layers defined via extrusion of a thermoplastic filament through a heated single-point nozzle	Utilizes a dispensing unit to deposit small volumes of liquid material that defines a 2D layer
Voxel-by-voxel raster scanning?	✓	✓	×	*Entire volume at once*	✓	✓	×
Limitations	• Requires complicated precise alignment, • Requires expensive high-power Femtosecond Laser • Time-consuming to scale to larger (cm-scale) areas	• Requires coating system for highly viscous material inks, • Complexity in multi-material printing • Geometric Constraints (i.e., overhangs require support structures)		• Complex process parameters, • Still in infancy • Ink must allow significant light penetration, low scattering	• Resolution constrained by nozzle diameter, • Not suitable for low-viscosity material • Geometric constraints (i.e., overhangs require support material)	• Low surface finish, • Low interfacial bonding quality, • Geometric constraints (i.e., overhangs require support material or structures)	• Restricted to very low-viscosity inks • Geometric constraints (i.e., overhangs require support material)
Feedstock	• Thermoset photo-curable monomers (Requirement) • Pertinent chemical functional groups listed in Table 2 • Functional fillers*				• Viscoelastic fluids, thermosets, & solvent-diluted thermoplastic polymers, • Functional Fillers*	• Thermoplastic polymers • Functional fillers*	• Ink Fluid Base • Aqueous • Solvent • Oil • Thermoset monomers • Functional Fillers*
Viscosity range	<10 Pa·s[99]			> 12 mPa·s[61] & >10 Pa·s[128]**	1 Pa·s–1350 Pa·s[99]	~200 Pa·s***[129] (molten/softened state)	<30 mPa-s[102]
Print resolution (dependencies) *X–Y*	Voxel size (nm-scale)	Laser spot size	Optical setup	Optical setup	Nozzle diameter		Droplet volume (picoliter-scale)
Print resolution (dependencies) *Z*		Light absorption	Light absorption		User-defined < Layer height < Nozzle diameter		
Special additional feedstock qualities	• Photoinitiator system (light-reactive element), Dye, and polymerization inhibitors control curing depth and overall reactivity of ink. • Optical Properties of embedded fillers (absorption/scatting) will affect *X–Y* and *Z* resolutions				Non-Newtonian Shear thinning	Non-Newtonian Shear thinning (molten/softened state)	1 < Z < 10**** • Z = 1/Oh • Oh = $\frac{\sqrt{We}}{Re} = \frac{\eta}{\sqrt{\gamma\rho L}}$ 6,102

*Functional Fillers—0D (spherical), 1D (fiber, short or continuous) or 2D (planar) particles of ceramic, metal, carbon, and biological materials.

**Higher-viscosity inks are preferred, but VAM has been shown to work with lower viscosity inks.

***General printability and good inter-raster bonding. This is the value at the intended printing extruder temperature and shear rate.

****General range of droplet formation in Droplet-on-Demand Inkjet Printing. The upper value can be larger. Oh is the Ohnesorge number, We is the Weber number, Re is the Reynolds number. η is the ink viscosity, γ is the ink surface tension, ρ is the ink density, and *L* is the characteristic length which can be the nozzle diameter of the printhead.

Resolution limitations would also include the resolution of system motion stages, which is not stated in the table.

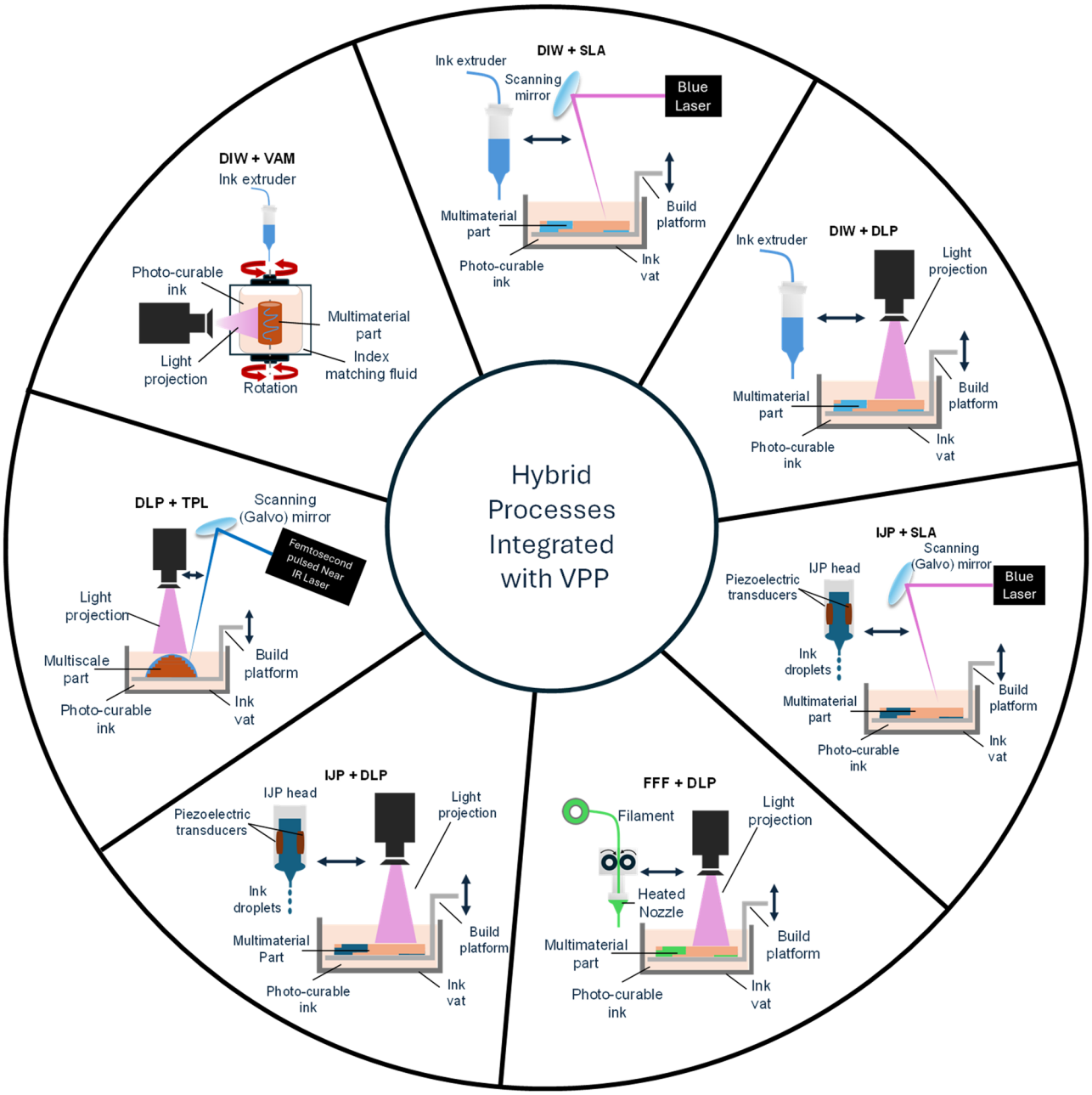

Fig. 5 | Schematic representations of different hybrid processes integrated with VPP.

However, the Z-resolution disparity between DIW and DLP necessitates printing multiple DLP layers for each DIW layer[103]. For reference, it has been demonstrated that DLP projectors can achieve a consistently reproducible resolution of 6 μm, underscoring their capacity for generating high-resolution features with intricate geometries[49]. Rau et al. expanded the range of printable materials to include those with viscosities up to 1350 Pa·s via DIW, surpassing the 10 Pa·s limits of traditional DLP alone, also demonstrating the fabrication of parts with the highest particle loadings (85 wt.%). DIW's deposition of conductive inks in combination with DLP's unique ability to create functional gradients through varied curing degrees via grayscale projections offers additional design flexibility, as illustrated by Chen et al.[108]. They developed a multi-level triboelectric generator (Fig. 6d) by manipulating crosslinking degrees to produce variable elastic moduli and, consequently, diverse electrical responses. Further advancing hybrid technology, Peng et al. produced free-standing Liquid Crystal Elastomer (LCE) meshes supported vertically by DLP-printed structures using laser-assisted DIW to print shape-retaining LCEs (Fig. 6e), enhancing actuation properties by aligning the LCE's mesogens through intentional stretching and in situ curing during extrusion[106]. This technique facilitated 4D printing of LCEs with tremendous potential applications in soft robotics, smart structures, active metamaterials, and smart wearable devices. Unlike the discussed hybrid technologies above where the integrated VPP modules were Top-down orientations, Jin et al. combined Bottom-up SLA with DIW, enabling unobstructed laser access during material dispensing[105]. This method is notable for dispensing DIW materials directly into the ink present in the vat and using multiple UV exposures to affix the DIW ink to the part being built on the inverted build platform. Dispensing ink directly into the vat for hybridized printing benefits from the vat ink's surface tension, aiding shape retention of the DIW deposited ink and overcoming the oxygen inhibition effect that could otherwise impair interlayer adhesion in Top-down systems. In another work, Riffe et al. used DIW to print the MeHA (methacrylated hyaluronic acid) suspension into the material matrix of GelMA (Gelatin methacrylamide), and obtained the multi-material part through single printing with VAM process. This study introduces the

Table 5 | Summary of VPP hybridization with other 3D printing modalities

Combined technologies	Advantages of combining technologies	Important highlights	Req. manual intervention?	Applications	References
SLA + DIW	Functional structure fabrication with diverse inks and materials, including shape memory polymers, magnetoactive soft materials, liquid elastomers, and conductive inks (DIW) featuring intricate details and complex geometry (SLA).	Exchange of parts between DIW and SLA system	Yes	Embedded circuitry	130
		First reported process that does not switch parts between systems, though it still requires pausing to clean substrates and insert electrical components.		Embedded electronic circuit, monolithic 3D packages	111
DLP + FFF	Creating bulk structure of specific mechanical, biological, and thermal properties (FFF) with detailed features or functional materials (DLP)	Though the fabrication approach is hybrid, overall systems are separate, as parts were printed separately using FFF and DLP methods.		Bio-scaffold with HA slurry	116
SLA + IJP	Local precise placement of functional material (IJP) into the substrate part (SLA)	Thermally stable SLA ink endured the high temperatures needed for piezopolymer annealing during post-processing.		Piezopolymer-based inertial sensor	113
DLP + DIW	Produce higher-resolution parts (DLP) from high-viscosity materials (DIW). Expand photo-curable ink use to include varied chemistries and increased molecular weights and particle/composite loadings.	Separate printing and manual assembly for full sensor integration		Sensors	107
		Used laser-assisted DIW to preserve the shape and functionality of the deposited LCE, stretching it during deposition to enhance actuation capabilities.	Fully automated	4D printing of LCEs, potential applications in soft robotics, smart structures, active metamaterials, and smart wearable devices	106
		Printed multiple DLP layers per DIW layer due to resolution disparities.		Multi-color parts, strain sensor, soft robots	103
		Expanded materials library for viscosities up to 1350 Pa·s, enabling printing with up to 85 wt.% particle loading.		Parts printed with sharp features despite high viscosity material	99
		DLP-assisted varying curing degrees across locations introduced functional gradients, enabling multi-level electrical responses.		Integrated mTENG in footwear soles to harvest energy from body motion and monitor motion state, creating functional wearable electronics.	108
SLA + DIW	*See previously mentioned "SLA + DIW"*	Implemented a bottom-up process where DIW material is deposited within the matrix and photo-cured via double or triple exposure to attach the deposited ink to an inverted building platform.		Multi-material ant, multi-material wheel, strain sensor	105
VAM + DIW	DIW prints suspension in the material matrix to achieve multi-material parts	Sacrificial gelatin material usage to modulate the viscosity of bioinks for 3D suspension prints of soft hydrogels		Tissue engineering, regenerative medicine	68
SLA + IJP	*See previously mentioned "SLA + IJP"*	Controlled drug release kinetics by strategically positioning the drug or a drug depot with a gradient from the inside to the outside.		Drug delivery	112
DLP + IJP	Depositing functional materials (IJP) onto the substrate (DLP)	Showcased the ability to create interconnected multi-layer electronic circuits in 3D structures.		Green part (before sintering), embedded circuit	114
SLA + AJP	Aerosol jet enables deposition of significantly higher-viscosity materials than inkjet printing (10–1000 mPa·s)	Replaced the SLA ink vat with a substrate (Bottom-up), mixing materials on-the-fly for specific compositions, unlike traditional bath-based SLA.		Cylindrical multi-material body with graduated material combination change	95,115
DLP + EHD jetting	Directly printed high resolution (~ 2.6 μm) functional pixels (EHD jetting) onto DLP substrates/frames.	Eliminated need for extra thermal annealing/drying, enabling direct printing of transparent OLED pixels onto 3D structures at high resolution in ambient conditions.		Transparent OLEDs	118
VPP + BJT + IJP + DIW + FFF	Multi-functional parts, functionally gradient parts, multi-color parts, multi-material parts.	System combined different processes, but demonstrated parts were only produced using VPP and paste extrusion.		N/A	119
DLP + TPL	Scalable features (DLP) with microscale precision capabilities (TPL) significantly reduces production time.	Requires precise/difficult alignment pre-setup due to higher precision of both TPL and DLP		Hierarchical superhydrophobic surfaces; aspherical microlens Composite of microlens & microfluidics	117

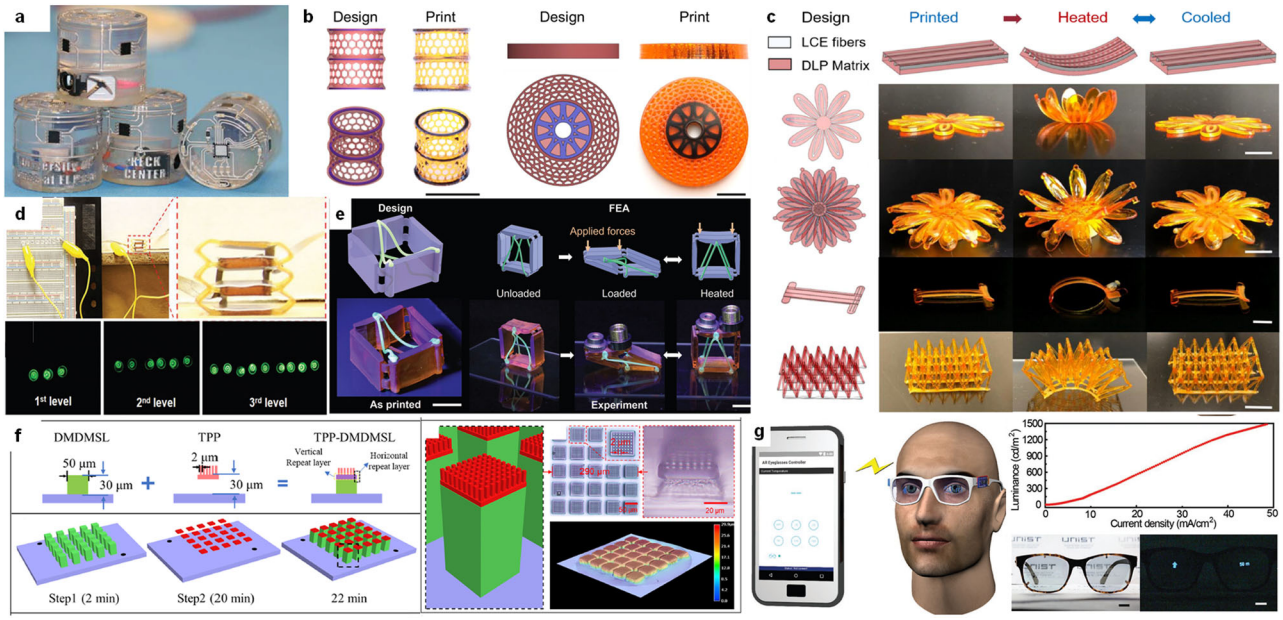

Fig. 6 | Functional devices fabricated by multiple printing modalities hybridized with VPP. a Example of 3D structural electronics printed with SLA and DIW (Image reproduced with permission from ref. 111, Copyright Emerald Publishing Limited, 2012). **b** Hybrid printed (DLP and DIW) multi-color prototypes (Image reproduced with permission from ref. 103, Copyright Elsevier, 2021). **c** Hybrid (DIW and DLP) printed soft robots using LCE fibers as active layers.(Image reproduced with permission from ref. 103, Copyright Elsevier, 2021). **d** Multi-level Triboelectric Nanogenerator (mTENG) printed with DIW and DLP is used to harvest energy to lighten LEDs where it can lighten 3, 6, and 9 LEDs by compression with first, second and third level of deformation. (Image reproduced with permission from ref. 108, Copyright John Wiley & Sons, Inc., 2019). **e** Hybrid printed (DLP + DIW) structure with tunable structural stability. Scale bar is 10 mm. (Image reproduced with permission from ref. 106, Copyright John Wiley & Sons, 2022). **f** Demonstration of superhydrophobic surface printing process and results with multi-scale features printed with DLP and TPL (Image reproduced with permission from[117], Copyright Elsevier, 2022). **g** Application of 3D-printed (EHD and DLP) transparent OLEDs as augmented reality eyeglasses with demonstration of turn-off (left) and turn-on (right) condition. Scale bar is 5 mm. (Image reproduced with permission from ref. 118, Copyright John Wiley & Sons, Inc., 2019).

innovative use of gelatin as a sacrificial material to modulate the viscosity of bioinks, enabling the VAM of low-viscosity materials such as soft hydrogels[68].

Another category of VPP hybridization technologies merges IJP with various VPP patterning methods. Konasch et al. explored a combination of SLA with IJP for drug delivery systems, where the inkjet method deposited active pharmaceutical ingredients into the SLA-printed structural components[112]. Similarly, a piezopolymer-based inertial sensor was developed by using IJP to pattern functional layers while employing SLA to print the primary structure[113]. Muguruza et al. integrated Top-down DLP with dual inkjet heads for embedded electronic circuits fabrication[114]. Hohnholz et al. opted for AJP over inkjet heads, benefiting from its ability to handle higher-viscosity materials[115]. On top of that, replacing the ink vat with a deposition substrate allowed for on-the-fly mixing of material to obtain various compositions, offering a flexible alternative compared to the fixed compositions in bath-based SLA systems.

While VPP has predominantly been combined with IJP or DIW technologies, it has also been integrated with other technologies to broaden its applications. Cheng et al. combined FFF with DLP in a sequential process to create bio-scaffolds from Hydroxyapatite (HA) slurry, using DLP for struts and FFF for molds to deposit the HA[116]. While not a singular automated hybrid system, this method represents a hybrid approach to manufacturing. In another innovation, TPL was combined with DLP to enhance production efficiency and enable fabrication of complex parts unachievable by either process alone[117]. TPL provided micron-scale precision, while DLP-printed large scalable features. This synergy facilitated the creation of composites with varied scales, such as microlenses integrated with microfluidics, and hierarchical superhydrophobic surfaces (Fig. 6f). Furthermore, An et al. explored the integration of EHD jetting with DLP to achieve high-resolution OLED pixels on 3D mechanical frames (Fig. 6g), demonstrating a novel approach to freeform optoelectronics without requiring vacuum deposition or etching[118]. Wagner et al. developed a multi-tool 3D Printing system that integrates a broad array of 3D printing technologies—BJT, IJP, VPP, DIW, and FFF into a singular integrated platform[119]. While this system offers versatility, practical application challenges exist related to material feedstock compatibility and variations in printing paths. The practical application was demonstrated only through the combination of DIW and VPP, hinting at additional complexities. Further assessments on hybrid parts using these technologies simultaneously have not been reported.

Integrating VPP with other 3D printing technologies highlights a path toward advancing the freeform manufacturing of functional devices while overcoming individual process hurdles. While significant material-related integration challenges associated with VPP hybridization have been identified, there are additional systematic challenges, which need to be considered. One such challenge is managing the complexities of the control system for multiple processes. This includes creating unified coordinate systems and standardized input commands. Some printing processes, like DIW and SLA, operate via single-voxel deposition and curing, respectively, and require toolpath commands. Other processes, such as IJP and DLP, operate via area-wise deposition and curing, respectively, and require image input commands. Moreover, the adoption of hybrid systems can lead to increased development and equipment costs as well as larger equipment footprints. Addressing these challenges is essential for harnessing the full potential of hybrid 3D printing technologies and extending applications.

Remaining challenges and outlook

Since the inception of multi-material VPP at the beginning of the 21st century, three distinct approaches to material switching have emerged within the VPP framework: (1) Multiple Vat Switching, (2) Single Vat with Dynamic Fluid Delivery, and (3) Unpatterned Ink Deposition "Vat-Less" VPP. In each of these approaches, significant reductions in the overall material switching times have been realized, with reported times much more

feasible for rapid functional device fabrication. However, challenges persist across all approaches, including material waste during the material switching process and scalability issues, particularly concerning large areas. It should be noted that rapid switching of 100 s of cm^2 build area multi-material VPP has been demonstrated within the last 5 years by Matte et al. and Cheng et al.[65,79]. In addition, solvent usage for cleaning high-viscosity inks mid-print can have detrimental effects on the final product. VPP has additionally been explored for hybridization with other 3D printing methods, expanding the range of materials that can be processed, thereby enhancing the versatility of functional device fabrication. Nevertheless, this hybridization approach presents its own set of challenges, including material compatibility, elevated equipment development costs, and larger system footprints resulting from the integration of multiple printing modalities.

Several opportunities for future work exist in multi-material VPP and VPP hybridization. (1) Material reclamation/recycling. This item can be extended to standard, single-material VPP as well. Material reclamation/recycling, generally, in VPP is uncommon. Printing the intended design and washing away the excess uncured material ink via a solvent is considered "Standard Operating Procedure". In fact, commercial single-material VPP systems will typically include "cleaning" accessories which include solvent baths and agitation such as: FormLabs' "Form Wash" or Carbon's "Smart Part Washer". The combined uncured ink and solvent waste would then be collected and sent to waste disposal. In more recent years, centrifugal acceleration has been utilized for material removal without the use of solvents, especially in more industrial settings. Carbon utilizes centrifugal cleaning where possible, and the centrifugal cleaning device additionally has a port for collecting removed ink for recycling[120]. Similarly, RapidShape's automated system for in-sequence production termed "RS Inline" also uses centrifugal cleaning method for material removal/recycling and claims that 90% of the uncured material is recovered[121]. In multi-material VPP, uncured ink is cleaned from the printed object during material switching predominantly via solvents, physical wiping, pressurized air jetting, or by flushing out the previous material ink with the new material ink. This can lead to significant amounts of wasted material, especially for large-area printed objects. Cheng et al. do utilize the centrifugal removal method to clean samples without solvent usage when switching materials in multi-material VPP[65]. It is not noted in the work if materials are recycled after cleaning, however. While the process is slower, Quero et al. notes collecting materials from the singular vat prior to solvent cleaning between material ink switching steps. This approach does act to minimize waste generation in Single Vat multi-material VPP[89]. In order for multi-material VPP to become a more scalable, large-area process these reclamation/recycling efforts need to be more greatly emphasized. (2) Scalability of multi-material VPP. In recent years 100 s of cm^2-scale build area prints have been performed with rapid material switching times. Can this be further scaled to full m^2-scale build areas? Having a larger-sized system in addition to efficient usage of prepared material inks can enable even larger area scalability to occur. (3) Further fundamental studies on process and feedstock interactions in VPP hybridization. Each standalone 3D printing modality has a preferred feedstock type and optimal processing parameters. Hybridization within 3D printing, generally, is a recent fabrication approach. When printing modalities are combined, new interactions occur with the various feedstocks (i.e., diffusion, adhesion, etc.) and process interactions (i.e., input energy, temperature, system layout, etc.). These interactions require further study to enable optimal processing and proper integration of the systems. Deposition processes integrate well (MJT and MEX), whereas build chamber processes (BJT, PBF, and VPP) are more challenging to integrate. The illumination mechanism for VPP (laser beam, digital light projector) can be integrated into larger hybrid assemblies. Controlled illumination combined with deposition requires further study.

Data availability

No datasets were generated or analysed during the current study.

Received: 9 May 2024; Accepted: 22 August 2024;
Published online: 06 November 2024

References

1. Calignano, F. et al. Overview on additive manufacturing technologies. *Proc. IEEE* **105**, 593–612 (2017).
2. Wehner, M. et al. An integrated design and fabrication strategy for entirely soft, autonomous robots. *Nature* **536**, 451–455 (2016).
3. ISO/ASTM: ISO/ASTM 52900:2001 (E). In *Additive manufacturing—General principles —Fundamentals and vocabulary* (ASTM International, ASTM International, West Conshohocken, PA, 2021).
4. Additive, G. New Manufacturing Milestone: 30,000 additive fuel nozzles. https://www.ge.com/additive/stories/new-manufacturing-milestone-30000-additive-fuel-nozzles (2018).
5. Vaezi, M., Seitz, H. & Yang, S. A review on 3D micro-additive manufacturing technologies. *Int. J. Adv. Manuf. Technol.* **67**, 1721–1754 (2013).
6. Nayak, L., Mohanty, S., Nayak, S. K. & Ramadoss, A. A review on inkjet printing of nanoparticle inks for flexible electronics. *J. Mater. Chem. C.* **7**, 8771–8795 (2019).
7. Appuhamillage, G. A. et al. 110th anniversary: vat photopolymerization-based additive manufacturing: current trends and future directions in materials design. *Ind. Eng. Chem. Res.* **58**, 15109–15118 (2019).
8. Bahati, D., Bricha, M. & El Mabrouk, K. Vat photopolymerization additive manufacturing technology for bone tissue engineering applications. *Adv. Eng. Mater.* **25**, 2200859 (2023).
9. Carbon: Introducing Adidas 4DFWD. https://www.carbon3d.com/resources/case-study/introducing-adidas-4dfwd-the-worlds-first-3d-printed-anisotropic-lattice-midsole-designed-to-move-you-forward (2021).
10. Carbon: Riddell Partners with Carbon® to Produce First-Ever 3D Printed Football Helmet Liner. https://www.carbon3d.com/news/press-releases/riddell-carbon-produce-football-helmet (2024).
11. Zhang, F. et al. The recent development of vat photopolymerization: a review. *Addit. Manuf.* **48**, 102423 (2021).
12. Layani, M., Wang, X. & Magdassi, S. Novel materials for 3D printing by photopolymerization. *Adv. Mater.* **30**, 1706344 (2018).
13. Tehfe, M. A., Louradour, F., Lalevée, J. & Fouassier, J.-P. Photopolymerization reactions: On the way to a green and sustainable chemistry. *Appl. Sci.* **3**, 490–514 (2013).
14. Bártolo, P. J. *Stereolithography: Materials, Processes and Applications* (Springer Science & Business Media, 2011).
15. Halloran, J. W. Ceramic stereolithography: additive manufacturing for ceramics by photopolymerization. *Annu. Rev. Mater. Res.* **46**, 19–40 (2016).
16. Zhang, S., Li, M., Hao, N. & Ragauskas, A. J. Stereolithography 3D printing of lignin-reinforced composites with enhanced mechanical properties. *ACS omega* **4**, 20197–20204 (2019).
17. Chen, X. et al. The development of an all-polymer-based piezoelectric photocurable resin for additive manufacturing. *Procedia CIRP* **65**, 157–162 (2017).
18. Song, X. et al. Piezoelectric component fabrication using projection-based stereolithography of barium titanate ceramic suspensions. *Rapid Prototyp. J.* **23**, 44–53 (2017).
19. Shao, G. et al. 3D printed magnetically-actuating micro-gripper operates in air and water. *Addit. Manuf.* **38**, 101834 (2021).
20. Lu, L., Guo, P. & Pan, Y. Magnetic-field-assisted projection stereolithography for three-dimensional printing of smart structures. *J. Manuf. Sci. Eng.* **139**, 071008 (2017).
21. Lu, L., Zhang, Z., Xu, J. & Pan, Y. 3D-printed polymer composites with acoustically assembled multidimensional filler networks for accelerated heat dissipation. *Compos. Part B: Eng.* **174**, 106991 (2019).
22. Huang, J., Qin, Q. & Wang, J. A review of stereolithography: processes and systems. *Processes* **8**, 1138 (2020).

23. Ware, H. O. T., Hai, R. & Sun, C. Vat photopolymerization. In *Springer Handbook of Additive Manufacturing* (eds Pei, E. et al.) 349–370 (Springer, 2023).
24. Hull, C. W. Method for production of three-dimensional objects by stereolithography. Google patents (U.S. Patent 4,929,402, 1990).
25. Hull, C. W. Apparatus for production of three-dimensional objects by stereolithography. Google patents (United States Patent, Appl., No. 638905, Filed, 1986).
26. Gibson, I. et al. Vat photopolymerization processes. In: *Additive Manufacturing Technologies: 3d Printing, Rapid Prototyping, and Direct Digital Manufacturing*. 63–106 (Springer, New York, NY, 2015).
27. Ge, Q. et al. Projection micro stereolithography based 3D printing and its applications. *Int. J. Extrem. Manuf.* **2**, 022004 (2020).
28. Sun, C., Fang, N., Wu, D. & Zhang, X. Projection micro-stereolithography using digital micro-mirror dynamic mask. *Sens. Actuators A: Phys.* **121**, 113–120 (2005).
29. Ware, H. O. T. & Sun, C. Method for attaining dimensionally accurate conditions for high-resolution three-dimensional printing ceramic composite structures using MicroCLIP process. *J. Micro Nanomanuf.* **7**, 031001 (2019).
30. Nguyen, A. K. & Narayan, R. J. Two-photon polymerization for biological applications. *Mater. Today* **20**, 314–322 (2017).
31. Harinarayana, V. & Shin, Y. Two-photon lithography for three-dimensional fabrication in micro/nanoscale regime: a comprehensive review. *Opt. Laser Technol.* **142**, 107180 (2021).
32. Pawlicki, M., Collins, H. A., Denning, R. G. & Anderson, H. L. Two-photon absorption and the design of two-photon dyes. *Angew. Chem. Int. Ed.* **48**, 3244–3266 (2009).
33. Wu, S., Serbin, J. & Gu, M. Two-photon polymerisation for three-dimensional micro-fabrication. *J. Photochem. Photobiol. A: Chem.* **181**, 1–11 (2006).
34. Zhou, X., Hou, Y. & Lin, J. A review on the processing accuracy of two-photon polymerization. *Aip Adv.* **5**, 3 (2015).
35. Fischer, J. & Wegener, M. Three-dimensional optical laser lithography beyond the diffraction limit. *Laser Photonics Rev.* **7**, 22–44 (2013).
36. Kuang, X. et al. Grayscale digital light processing 3D printing for highly functionally graded materials. *Sci. Adv.* **5**, eaav5790 (2019).
37. Ge, Q. et al. 3D printing of highly stretchable hydrogel with diverse UV curable polymers. *Sci. Adv.* **7**, eaba4261 (2021).
38. Yue, L. et al. Single-vat single-cure grayscale digital light processing 3D printing of materials with large property difference and high stretchability. *Nat. Commun.* **14**, 1251 (2023).
39. Hahn, V. et al. Rapid assembly of small materials building blocks (voxels) into large functional 3D metamaterials. *Adv. Funct. Mater.* **30**, 1907795 (2020).
40. Saha, S. K. et al. Scalable submicrometer additive manufacturing. *Science* **366**, 105–109 (2019).
41. van Lith, R, Baker, E. et al. 3D-printing strong high resolution antioxidant bioresorbable vascular stents. *Adv. Mater. Technol.* https://doi.org/10.1002/admt.201600138 (2016).
42. Tumbleston, J. R. et al. Continuous liquid interface production of 3D objects. *Science* **347**, 1349–1352 (2015).
43. Janusziewicz, R., Tumbleston, J. R., Quintanilla, A. L., Mecham, S. J. & DeSimone, J. M. Layerless fabrication with continuous liquid interface production. *Proc. Natl. Acad. Sci. USA* **113**, 11703–11708 (2016).
44. Carbon, I. 3D printing materials for real-world applications. https://www.carbon3d.com/materials (2024).
45. Wang, W. et al. High-speed and high-resolution 3D printing of self-healing and ion-conductive hydrogels via μCLIP. *ACS Mater. Lett.* **5**, 1727–1737 (2023).
46. Ware, H. et al. In situ formation of micro/nano phase composite for 3D printing clinically relevant bioresorbable stents. *Mater. Today Chem.* **26**, 101231 (2022).
47. Keate, R. L. et al. 3D-printed electroactive hydrogel architectures with sub-100 μm resolution promote myoblast viability. *Macromol. Biosci.* **22**, 2200103 (2022).
48. Liu, L., Liu, S., Schelp, M. & Chen, X. Rapid 3D printing of bioinspired hybrid structures for high-efficiency fog collection and water transportation. *ACS Appl. Mater. Interfaces* **13**, 29122–29129 (2021).
49. Hsiao, K. et al. Single-digit-micrometer-resolution continuous liquid interface production. *Sci. Adv.* **8**, eabq2846 (2022).
50. Shao, G., Hai, R. & Sun, C. 3D printing customized optical lens in minutes. *Adv. Opt. Mater.* **8**, 1901646 (2020).
51. Ding, Y. et al. 3D-printed radiopaque bioresorbable stents to improve device visualization. *Adv. Healthc. Mater.* **11**, 2201955 (2022).
52. Walker, D. A., Hedrick, J. L. & Mirkin, C. A. Rapid, large-volume, thermally controlled 3D printing using a mobile liquid interface. *Science* **366**, 360–364 (2019).
53. Azul 3D. https://www.azul3d.com/ (2023).
54. De Beer, M. P. et al. Rapid, continuous additive manufacturing by volumetric polymerization inhibition patterning. *Sci. Adv.* **5**, eaau8723 (2019).
55. Lin, W. et al. Enhanced continuous liquid interface production with track-etched membrane. *Rapid Prototyp. J.* **25**, 117–125 (2019).
56. Van Der Laan, H. L., Burns, M. A. & Scott, T. F. Volumetric photopolymerization confinement through dual-wavelength photoinitiation and photoinhibition. *ACS Macro Lett.* **8**, 899–904 (2019).
57. Kelly, B. E. et al. Volumetric additive manufacturing via tomographic reconstruction. *Science* **363**, 1075–1079 (2019).
58. Loterie, D., Delrot, P. & Moser, C. High-resolution tomographic volumetric additive manufacturing. *Nat. Commun.* **11**, 852 (2020).
59. Toombs, J. T. et al. Volumetric additive manufacturing of silica glass with microscale computed axial lithography. *Science* **376**, 308–312 (2022).
60. Bhattacharya, I., Toombs, J. & Taylor, H. High fidelity volumetric additive manufacturing. *Addit. Manuf.* **47**, 102299 (2021).
61. Thijssen, Q., Toombs, J., Li, C. C., Taylor, H. & Van Vlierberghe, S. From pixels to voxels: a mechanistic perspective on volumetric 3D-printing. *Progr. Polymer Sci.* **147**, 101755 (2023).
62. Zheng, X. Y. et al. Multiscale metallic metamaterials. *Nat. Mater.* **15**, 1100–1106 (2016).
63. Emami, M. M., Barazandeh, F. & Yaghmaie, F. Scanning-projection based stereolithography: method and structure. *Sens. Actuat A-Phys.* **218**, 116–124 (2014).
64. Meenakshisundaram, V., Sturm, L. D., Williams, C. B. Modeling a scanning-mask projection vat photopolymerization system for multiscale additive manufacturing. *J. Mater. Process. Technol.* **279**, 116546 (2020).
65. Cheng, J. et al. Centrifugal multimaterial 3D printing of multifunctional heterogeneous objects. *Nat. Commun.* **13**, 7931 (2022).
66. Lipkowitz, G. et al. Injection continuous liquid interface production of 3D objects. *Sci. Adv.* **8**, eabq3917 (2022).
67. Maruo, S., Ikuta, K. & Ninagawa, T. Multi-polymer microstereolithography for hybrid opto-MEMS. In *Technical Digest. MEMS 2001. 14th IEEE International Conference on Micro Electro Mechanical Systems (Cat. No. 01CH37090)* 151–154 (IEEE, 2001).
68. Riffe, M. B. et al. Multi-material volumetric additive manufacturing of hydrogels using gelatin as a sacrificial network and 3D suspension bath. *Adv. Mater.* **36**, 2309026 (2024).
69. Xu, W. et al. 3D printing-enabled nanoparticle alignment: a review of mechanisms and applications. *Small* **17**, 2100817 (2021).
70. Wang, Z., Guo, Y., Cai, S. & Yang, J. Three-dimensional printing of liquid crystal elastomers and their applications. *ACS Appl. Polym. Mater.* **4**, 3153–3168 (2022).
71. Chen, J. et al. 3D-Printed anisotropic polymer materials for functional applications. *Adv. Mater.* **34**, 2102877 (2022).

72. Cui, H. et al. Design and printing of proprioceptive three-dimensional architected robotic metamaterials. *Science* **376**, 1287–1293 (2022).
73. Chen, D. & Zheng, X. Multi-material additive manufacturing of metamaterials with giant, tailorable negative Poisson's ratios. *Sci. Rep.* **8**, 1–8 (2018).
74. Ma, X. et al. Deterministically patterned biomimetic human iPSC-derived hepatic model via rapid 3D bioprinting. *Proc. Natl. Acad. Sci. USA* **113**, 2206–2211 (2016).
75. Wang, Z. et al. Charge-programmable photopolymers for 3D electronics via additive manufacturing. *Adv. Funct. Mater.* **34**, 2313839 (2024).
76. Wicker, R., Medina, F. & Elkins, C. Multiple material micro-fabrication: extending stereolithography to tissue engineering and other novel applications. In *2004 International Solid Freeform Fabrication Symposium* (Laboratory for Freeform Fabrication and University of Texas at Austin, 2004).
77. Arcaute, K., Zuverza, N., Mann, B. & Wicker, R. Multi-material stereolithography: spatially-controlled bioactive poly (ethylene glycol) scaffolds for tissue engineering. In *2007 International Solid Freeform Fabrication Symposium* (Laboratory for Freeform Fabrication and University of Texas at Austin, 2007).
78. Zhou, C., Chen, Y., Yang, Z. & Khoshnevis, B. Digital material fabrication using mask-image-projection-based stereolithography. *Rapid Prototyp. J.* **19**, 153–165 (2013).
79. Matte, C.-D., Pearson, M., Trottier-Cournoyer, F., Dafoe, A. & Kwok, T. H. Automated storage and active cleaning for multi-material digital-light-processing printer. *Rapid Prototyp. J.* **25**, 864–874 (2019).
80. Jiang, C.-P. et al. Design and fabrication of multi-material pneumatic soft gripper using newly developed high-speed multi-material vat photopolymerization 3D printer. *Int. J. Adv. Manuf. Technol.* **130**, 1093–1106 (2023).
81. Hu, K., Zhao, P., Li, J. & Lu, Z. High-resolution multiceramic additive manufacturing based on digital light processing. *Addit. Manuf.* **54**, 102732 (2022).
82. Huang, J., Ware, H. O. T., Hai, R., Shao, G. & Sun, C. Conformal geometry and multimaterial additive manufacturing through freeform transformation of building layers. *Adv. Mater.* **33**, 2005672 (2021).
83. Huang, P., Deng, D. & Chen, Y. Modeling and fabrication of heterogeneous three-dimensional objects based on additive manufacturing. In *ASME International Mechanical Engineering Congress and Exposition* p. V02AT02A056 (American Society of Mechanical Engineers, 2013).
84. Khatri, B., Frey, M., Raouf-Fahmy, A., Scharla, M.-V. & Hanemann, T. Development of a multi-material stereolithography 3D printing device. *Micromachines* **11**, 532 (2020).
85. Choi, J.-W., Kim, H.-C. & Wicker, R. Multi-material stereolithography. *J. Mater. Process. Technol.* **211**, 318–328 (2011).
86. Inamdar, A., Magana, M., Medina, F., Grajeda, Y. & Wicker, R. Development of an automated multiple material stereolithography machine. In *2006 International Solid Freeform Fabrication Symposium* (Laboratory for Freeform Fabrication and University of Texas at Austin, 2006).
87. Miri, A. K. et al. Microfluidics-enabled multimaterial maskless stereolithographic bioprinting. *Adv. Mater.* **30**, 1800242 (2018).
88. Han, D., Yang, C., Fang, N. X. & Lee, H. Rapid multi-material 3D printing with projection micro-stereolithography using dynamic fluidic control. *Addit. Manuf.* **27**, 606–615 (2019).
89. Quero, R. F., de Jesus, D. P. & da Silva, J.A.F. Simple modification to allow high-efficiency and high-resolution multi-material 3D-printing fabrication of microfluidic devices. *Lab Chip* **23**, 3694–3703 (2023).
90. Maruyama, T., Hirata, H., Furukawa, T. & Maruo, S. Multi-material microstereolithography using a palette with multicolor photocurable resins. *Opt. Mater. Express* **10**, 2522–2532 (2020).
91. Wang, Q. et al. Lightweight mechanical metamaterials with tunable negative thermal expansion. *Phys. Rev. Lett.* **117**, 175901 (2016).
92. Kowsari, K., Akbari, S., Wang, D., Fang, N. X. & Ge, Q. High-efficiency high-resolution multimaterial fabrication for digital light processing-based three-dimensional printing. *3D Print. Addit. Manuf.* **5**, 185–193 (2018).
93. Yuan, C., Wang, F. & Ge, Q. Multimaterial direct 4D printing of high stiffness structures with large bending curvature. *Extrem. Mech. Lett.* **42**, 101122 (2021).
94. Zhang, Y. F. et al. Miniature pneumatic actuators for soft robots by high-resolution multimaterial 3D printing. *Adv. Mater. Technol.* **4**, 1900427 (2019).
95. Overmeyer, L., Hohnholz, A., Suttmann, O. & Kaierle, S. Multi-material laser direct writing of aerosol jet layered polymers. *CIRP Ann.* **68**, 217–220 (2019).
96. Lithoz America. CeraFabMulti 2M30 the multimaterial 3D printer. https://lithoz.com/en/3d-printer/cerafab-multi/ (2022).
97. Admatec Europe. The Admaflex technology. https://admateceurope.com/admaflex-technology (2020).
98. Admatec Europe. Admaflex 300 multi-material. https://admateceurope.com/admaflex300-multimaterial (2020).
99. Rau, D. A., Forgiarini, M. & Williams, C. B. Hybridizing direct ink write and mask-projection vat photopolymerization to enable additive manufacturing of high viscosity photopolymer resins. *Addit. Manuf.* **42**, 101996 (2021).
100. Komissarenko, D. A., Sokolov, P. S., Evstigneeva, A. D., Shmeleva, I. A. & Dosovitsky, A. E. Rheological and curing behavior of acrylate-based suspensions for the DLP 3D printing of complex zirconia parts. *Materials* **11**, 2350 (2018).
101. Saadi, M. et al. Direct ink writing: a 3D printing technology for diverse materials. *Adv. Mater.* **34**, 2108855 (2022).
102. Derby, B. Additive manufacture of ceramics components by inkjet printing. *Engineering* **1**, 113–123 (2015).
103. Peng, X. et al. Integrating digital light processing with direct ink writing for hybrid 3D printing of functional structures and devices. *Addit. Manuf.* **40**, 101911 (2021).
104. Zanjani, J. S. M. & Baran, I. Co-bonded hybrid thermoplastic-thermoset composite interphase: Process-microstructure-property correlation. *Materials* **14**, 291 (2021).
105. Jin, J. et al. Hybrid multimaterial 3D printing using photocuring-while-dispensing. *Small* **19**, 2302405 (2023).
106. Peng, X. et al. 4D printing of freestanding liquid crystal elastomers via hybrid additive manufacturing. *Adv. Mater.* **34**, 2204890 (2022).
107. Vatani, M., Lu, Y., Engeberg, E. D. & Choi, J.-W. Combined 3D printing technologies and material for fabrication of tactile sensors. *Int. J. Precis. Eng. Manuf.* **16**, 1375–1383 (2015).
108. Chen, K. et al. Dynamic photomask-assisted direct ink writing multimaterial for multilevel triboelectric nanogenerator. *Adv. Funct. Mater.* **29**, 1903568 (2019).
109. Palmer, J. A. et al. Realizing 3-D interconnected direct write electronics within smart stereolithography structures. In *ASME International Mechanical Engineering Congress and Exposition*. 287–293 (ASME, 2005).
110. Lopes, A. et al. Expanding rapid prototyping for electronic systems integration of arbitrary form. In *2006 International Solid Freeform Fabrication Symposium* (Laboratory for Freeform Fabrication and University of Texas at Austin, 2006).
111. Joe Lopes, A., MacDonald, E. & Wicker, R. B. Integrating stereolithography and direct print technologies for 3D structural electronics fabrication. *Rapid Prototyp. J.* **18**, 129–143 (2012).
112. Konasch, J. et al. Novel 3D printing concept for the fabrication of time-controlled drug delivery systems. *Curr. Dir. Biomed. Eng.* **4**, 141–144 (2018).
113. Bernasconi, R. et al. Hybrid additive manufacturing of a piezopolymer-based inertial sensor. *Addit. Manuf.* **59**, 103091 (2022).

114. Muguruza, A. et al. Development of a multi-material additive manufacturing process for electronic devices. *Procedia Manuf.* **13**, 746–753 (2017).
115. Hohnholz, A. et al. Multimaterial bathless stereolithography using aerosol jet printing and UV laser based polymerization. *J. Laser Appl.* **31**, 022301 (2019).
116. Cheng, Y.-J., Wu, T.-H., Tseng, Y.-S. & Chen, W.-F. Development of hybrid 3D printing approach for fabrication of high-strength hydroxyapatite bioscaffold using FDM and DLP techniques. *Biofabrication* **16**, 025003 (2024).
117. Tan, M. et al. Cross-scale and cross-precision structures/systems fabricated by high-efficiency and low-cost hybrid 3D printing technology. *Addit. Manuf.* **59**, 103169 (2022).
118. An, H. S. et al. High-resolution 3D printing of freeform, transparent displays in ambient air. *Adv. Sci.* **6**, 1901603 (2019).
119. Wagner, G. W. et al. Design and development of a multi-tool additive manufacturing system. In *2017 International Solid Freeform Fabrication Symposium* (University of Texas, Austin, 2017).
120. Carbon, I. Sustainable manufacturing: carbon's efforts to lead the way. https://www.carbon3d.com/resources/blog/sustainable-manufacturing-carbons-efforts-to-lead-the-way (2024).
121. RapidShape: Fully Automated System for Non Stop Production. https://www.rapidshape.de/portfolio-item/rs-inline-industry/ (2024).
122. Zhang, J. & Xiao, P. 3D printing of photopolymers. *Polym. Chem.* **9**, 1530–1540 (2018).
123. Formlabs. Formlabs Stereolithography 3D Printers Tech Specs. https://formlabs.com/3d-printers/resin/tech-specs/ (2024).
124. LLC, U. T. https://www.uniz.com/us_en/3d-printers/slash-2-plus. Slash 2 Plus, Uniz Technology LLC (2019).
125. Lu, Y. et al. Microstereolithography and characterization of poly (propylene fumarate)-based drug-loaded microneedle arrays. *Biofabrication* **7**, 045001 (2015).
126. Bhusal, A. et al. Multi-material digital light processing bioprinting of hydrogel-based microfluidic chips. *Biofabrication* **14**, 014103 (2021).
127. Wu, X., Lian, Q., Li, D. & Jin, Z. Biphasic osteochondral scaffold fabrication using multi-material mask projection stereolithography. *Rapid Prototyp. J.* **25**, 277–288 (2019).
128. Whyte, D. J., Doeven, E. H., Sutti, A., Kouzani, A. Z. & Adams, S. D. Volumetric additive manufacturing: a new frontier in layer-less 3D printing. *Addit. Manuf.* **84**, 104094 (2024).
129. Sola, A. Materials requirements in fused filament fabrication: a framework for the design of next-generation 3D printable thermoplastics and composites. *Macromol. Mater. Eng.* **307**, 2200197 (2022).
130. Medina, F. et al. Hybrid manufacturing: integrating direct write and stereolithography. In *2005 International Solid Freeform Fabrication Symposium* (Laboratory for Freeform Fabrication and University of Texas at Austin, 2005).

Acknowledgements

Work by Saroj Subedi, S. M. Abu Naser Shovon, and Henry Oliver T. Ware was funded by North Carolina State University (NCSU) startup funding. Work by Siying Liu, Wenbo Wang, and Xiangfan Chen was funded by Arizona State University (ASU) startup funding, the 2022 & 2023 Mayo Clinic and Arizona State University (ASU) Alliance for Health Care Collaborative ResearchSeed Grant Program, and National Science Foundation (NSF) Future Manufacturing (FM) Award (CMMI 2229279).

Author contributions

S.S. and S.L. contributed equally to this work by preparing key large sections of the manuscript, Figures, and Tabular information. W.W. prepared key section of the manuscript and Tabular information. S.M.A.N.S. prepared key sections of the manuscript and Tabular information. X.C. and H.O.T.W. prepared key sections of the manuscript, Figures, and Tabular information, and will act as Corresponding Authors. All authors reviewed the manuscript for submission.

Competing interests

The authors declare no competing interests.

Additional information

Correspondence and requests for materials should be addressed to Xiangfan Chen or Henry Oliver T. Ware.

Reprints and permissions information is available at http://www.nature.com/reprints

Publisher's note Springer Nature remains neutral with regard to jurisdictional claims in published maps and institutional affiliations.

Open Access This article is licensed under a Creative Commons Attribution-NonCommercial-NoDerivatives 4.0 International License, which permits any non-commercial use, sharing, distribution and reproduction in any medium or format, as long as you give appropriate credit to the original author(s) and the source, provide a link to the Creative Commons licence, and indicate if you modified the licensed material. You do not have permission under this licence to share adapted material derived from this article or parts of it. The images or other third party material in this article are included in the article's Creative Commons licence, unless indicated otherwise in a credit line to the material. If material is not included in the article's Creative Commons licence and your intended use is not permitted by statutory regulation or exceeds the permitted use, you will need to obtain permission directly from the copyright holder. To view a copy of this licence, visit http://creativecommons.org/licenses/by-nc-nd/4.0/.

© The Author(s) 2024